



HAL
open science

Geology, biostratigraphy and carbon isotope chemostratigraphy of the Palaeogene fossil-bearing Dakhla sections, southwestern Moroccan Sahara

Mouloud Benammi, Sylvain Adnet, Laurent Marivaux, Johan Yans, Corentin Noiret, Rodolphe Tabuce, Jérôme Surault, Imad El Kati, Sebastien Enault, Lahssen Baidder, et al.

► To cite this version:

Mouloud Benammi, Sylvain Adnet, Laurent Marivaux, Johan Yans, Corentin Noiret, et al.. Geology, biostratigraphy and carbon isotope chemostratigraphy of the Palaeogene fossil-bearing Dakhla sections, southwestern Moroccan Sahara. *Geological Magazine*, 2019, 156 (1), pp.117-132. 10.1017/S0016756817000851 . hal-01813156

HAL Id: hal-01813156

<https://hal.umontpellier.fr/hal-01813156>

Submitted on 1 Nov 2020

HAL is a multi-disciplinary open access archive for the deposit and dissemination of scientific research documents, whether they are published or not. The documents may come from teaching and research institutions in France or abroad, or from public or private research centers.

L'archive ouverte pluridisciplinaire **HAL**, est destinée au dépôt et à la diffusion de documents scientifiques de niveau recherche, publiés ou non, émanant des établissements d'enseignement et de recherche français ou étrangers, des laboratoires publics ou privés.

**Geology, biostratigraphy and carbon isotope
chemostratigraphy of the Paleogene fossil-bearing Dakhla
sections, Southwestern Moroccan Sahara**

Journal:	<i>Geological Magazine</i>
Manuscript ID	GEO-17-1733.R1
Manuscript Type:	Review Article
Date Submitted by the Author:	n/a
Complete List of Authors:	benammi, mouloud; Universite de Poitiers UFR Sciences Fondamentales et Appliquees, Institut de Paléoprimateologie et Paléontologie humaine: Evolution et Paléoenvironnements - iPHEP CNRS UMR 7262 Adnet, Sylvain; Universite de Montpellier, 2Institut des Sciences de l'Evolution de Montpellier (ISE-M), UMR 5554 CNRS/UM/IRD/EPHE Marivaux, Laurent; Universite de Montpellier, 2Institut des Sciences de l'Evolution de Montpellier (ISE-M), UMR 5554 CNRS/UM/IRD/EPHE Yans, Johan; Universite de Namur, Department of Geology Noiret, Corentin; Universite de Namur, Department of Geology Tabuce, rodolphe; Universite de Montpellier, 2Institut des Sciences de l'Evolution de Montpellier (ISE-M), UMR 5554 CNRS/UM/IRD/EPHE Surault, Jerome; Universite de Poitiers UFR Sciences Fondamentales et Appliquees, 1Institut International de Paléoprimateologie, Paléontologie Humaine: Evolution et Paléoenvironnements (iPHEP), UMR-CNRS 7262 El Kati, Imad; Universite Ibn Tofail Kenitra, 5Laboratoire de Géologie, Géophysique, Géorisques et environnement (3GE), Département de Géologie Enault, Sebastien; Universite de Montpellier, Institut des Sciences de l'Evolution de Montpellier (ISE-M), UMR 5554 CNRS/UM/IRD/EPHE Baidder, Lahcen; Universite Hassan II Casablanca, Laboratoire Géosciences Saddiqi, Omar; Universite Hassan II Casablanca, Laboratoire Géosciences Benammi, Mohamed; Universite Ibn Tofail Kenitra, 5Laboratoire de Géologie, Géophysique, Géorisques et environnement (3GE), Département de Géologie
Keywords:	Oligocene, southwestern Morocco, magnetostratigraphy, mammals, chemostratigraphy, biostratigraphy, rodents

1
2
3 1 Geology, biostratigraphy and carbon isotope chemostratigraphy of the
4 2 Paleogene fossil-bearing Dakhla sections, Southwestern Moroccan Sahara
5
6
7

8 **BENAMMI MOULOUD¹, ADNET SYLVAIN², MARIVAUX LAURENT², YANS**
9
10 **JOHAN³, NOIRET CORENTIN³, TABUCE RODOLPHE², SURAULT JÉRÔME¹, EL**
11
12 **KATI IMAD⁵, ENAULT SÉBASTIEN², BAIDDER LAHCEN⁴, SADDIQI OMAR⁴,**
13
14 **BENAMMI MOHAMED⁵**
15
16
17
18
19

20 9 ¹*Institut International de Paléoprimatologie, Paléontologie Humaine: Evolution et*
21

22 10 *Paléoenvironnements (iPHEP), UMR-CNRS 7262, Université de Poitiers UFR SFA, 40*
23
24 *avenue du Recteur Pineau, F-86022 Poitiers cedex, France*
25

26 12 ²*Institut des Sciences de l'Evolution de Montpellier (ISE-M), UMR 5554*
27

28 13 *CNRS/UM/IRD/EPHE, CC064, Université de Montpellier, place Eugène Bataillon, F-34095*
29
30 *Montpellier cedex 05, France*
31

32 15 ³*Department of Geology, University of Namur, rue de Bruxelles 61, 5000 Namur, Belgium*
33

34 16 ⁴*Laboratoire Géosciences, Université Hassan II-Casablanca, BP 5366 Maârif, Casablanca,*
35
36
37 *Morocco*
38

39 18 ⁵*Laboratoire de Géologie, Géophysique, Géorisques et environnement (3GE), Département de*
40
41 *Géologie, Université Ibn Tofail, Faculté des Sciences, BP. 133, Kenitra, Morocco*
42
43
44

45 20
46
47
48
49
50
51
52
53
54
55
56
57
58
59
60

21 **ABSTRACT**

22 Recently new Paleogene vertebrate localities were reported in the southern Dakhla **area**
23 (southwestern Morocco). The Eocene sediment strata crops out on cliffs along the Atlantic
24 Ocean coast. Vertebrate remains come from five conglomeratic sandstone beds and are
25 principally represented by isolated teeth belonging to micromammals, selachians and bony
26 fishes, a proboscidean assigned to *?Numidotherium* sp., and many remains of archaeocete
27 whales (Basilosauridae). During the fieldwork, five lithostratigraphic sections were described,
28 essentially based on the lithological characteristic of sediments. Despite the lateral variations
29 of facies, correlations between these five sections were possible on the basis of fossil-bearing
30 beds (A1, B1, B2, C1, and C2), and five lithological units were identified. The lower part of
31 the section consists of rhythmically-bedded, chert-rich marine siltstones and marls with thin
32 black phosphorite with organic matter at the base. The overlying units include coarse-grained
33 to microconglomeratic sandstones interbedded with silts, thereby indicating **deposition** in
34 shallow marine environment with fluvial influence. The natural remanence magnetization of a
35 total of 50 samples was measured, and the intensity of most of the samples is too weak, before
36 or after the first step of demagnetization. The paleomagnetic data of the samples are very
37 unstable, except eight from three **similar** sandstone levels, which show a normal polarity.
38 Matched with biostratigraphic data on **rodents, primates**, the selachian, sirenian and cetacean
39 faunas, the new carbon isotope chemostratigraphy on organics 1) refines the age of the
40 uppermost C2 fossil-bearing bed to the earliest Oligocene, and 2) confirms the Priabonian age
41 of the B1 to C1 **levels**.

42 **Keywords:** Oligocene, southwestern Morocco, magnetostratigraphy, mammals,
43 chemostratigraphy, biostratigraphy, rodents

44

1. Introduction

The study area is in south of Morocco, 60 km south the coastal town of Dakhla (Fig. 1). This area forms a part of the Tarfaya-Dakhla Basin. It is the southernmost Atlantic basin of Morocco, and extends from the Mauritania border in the south to the Canary Islands in the north. It stretches over more than 1000 km along the western margin of the Sahara, and covers an area of 170,000 km², both on- and off-shore (Davison, 2005; Sachse et al., 2011, 2014).

The geological and stratigraphic structures of the basin have been investigated in detail using well and seismic data (Kolonis et al., 2002, Klingelhoefer et al., 2009 and Davison & Dailly, 2010). The Tarfaya-Dakhla Basin is filled by Mesozoic and Cenozoic continental to shallow-marine sediments, which overlie the basement Precambrian and/or Paleozoic rocks.

The study area is located in the southern margin of the Tarfaya-Dakhla Basin, between latitude 22°50' and 24°05' N; a sector between the gulf of Cintra and N'Tireft village (Fig. 1).

The escarpment exposes Paleogene to Quaternary sediments, which have recently been notable for their abundant and diverse marine and terrestrial faunas, particularly vertebrates (Adnet et al., 2010, Zouhri et al., 2014, Benammi et al., 2014a, 2014b, Marivaux et al., 2017).

Paleontological data are also exploited by commercial fossil dealers and amateur fossil collectors, a situation which then deserves protection by the authorities as a geosite (Saddiqi et al., 2015).

This work, based on lithologic, paleomagnetic, carbon isotope chemostratigraphy and biochronological data, allows us to describe and refine the nature and age of the sedimentological deposits exposed in the Dakhla region, and notably to constrain the dating of its paleontological content (Paleogene faunas).

70 2. Geological setting

71 The studied Paleogene succession corresponds to the Samlat Formation (Fm.) of Ratschiller
72 (1967). It is exposed in different areas, notably cliffs along the Atlantic Ocean coast, and have
73 also been recognized in boreholes drillings (Ranke et al., 1982, Davison, 2005) on the
74 continental shelf. There have been few geological studies carried out on these units in the
75 Dakhla area (e.g. Ratschiller 1967; Ortlieb, 1975), **which were** inappropriately mapped as
76 Mio-Pliocene by Rjimati et al. (2008), and contrary to those devoted to deposits capping the
77 beach cliffs near Dakhla and dated to the Mio-Quaternary period (e.g. Joleaud, 1907; Front Y
78 Sague, 1911; Deperet, 1912; Lecointre 1962, 1966). In the framework of our geological and
79 paleontological program in the early Tertiary of North Africa, since 2013 we have carried out
80 researches in the westernmost part of the Sahara in Morocco, notably on the geological
81 outcrops of the Samlat Formation exposed between Garitas and about 60 km north of the
82 crossroad at the entrance of the Dakhla peninsula (Fig. 1a, b). Recent paleontological studies
83 in this region have yielded vertebrate fossils, which indicate that some of the deposits are late
84 Eocene in age (Adnet et al., 2010; Zouhri et al., 2014). New sedimentological, geochemical
85 and magnetostratigraphic studies were carried out, in order to **refine** the age of these
86 Paleogene deposits. Between 2013 and 2015, our field research **was** devoted to prospecting
87 the outcrops, in search of fossil-bearing levels. The escarpment prospected lies between lat.
88 22°51' to the south and lat. 24° to the north (in some zones **the** outcrops are covered by
89 modern sand dunes). About 150 km south of Dakhla, the thickness of the outcrops is reduced
90 and is only a few meters above sea level. It is only from Garitas and beyond to the north, that
91 the escarpment exposes Paleogene sediments, which are **notable** for their abundant and
92 diverse marine vertebrates.

93

94

95 3. Materials and methods

96 In order to reconstruct the past sedimentary environment, outcrops were sought in the Dakhla
97 peninsula and in the surrounding areas. For each outcrop, a number of sections were selected
98 for detailed study along the coastal cliffs. The succession of lithofacies was described from
99 the base to the top of the sequence for each section. The description was essentially based on
100 the lithological characteristic of sediments and the sedimentary structures. This description
101 enabled us to establish correlations between sections based on fossil-bearing levels as
102 previously reported in Adnet et al. (2010).

103 Field studies included selection of different outcrops with easy access; we measured five
104 stratigraphic sequences, bed by bed, with Jacob Staff. These sections are located about 50 km
105 south of Dakhla. In addition, a paleomagnetic study was carried out along the Porto Rico
106 section (Fig. 1). A total of 29 cores were drilled in the field from 13 distinct levels with a
107 portable gasoline powered drill, and oriented in situ with a magnetic compass. Most sites
108 drilled correspond to the Unit 2 and the lower part of Unit 3 (see below). The lithology
109 sampled includes sandstones, clays and silts.

110 Carbon isotope analyses were performed on 43 samples (Table 1) of the Porto Rico (Pto) and
111 El Argoub (Arg) sections. Organic matter of the sediments was isolated, following the
112 procedure described in Yans et al. (2010) and refined by Storme et al. (2012). The bulk
113 organic carbon isotope analyses ($\delta^{13}\text{C}_{\text{org}}$) are based on powdered rock samples of about 1 to
114 10 g, acidified in 25% HCl solution for two hours in order to remove carbonate. The
115 numerous carbonate-free samples were treated similarly. Soluble salts were removed by
116 repetitive (1-10) centrifuging (4000 revolutions per minute) with deionized water until a
117 neutral sediment was obtained. Finally, residues were dried at 35°C and powdered again.
118 Carbon isotope analysis of organic carbon was performed with an elemental analyzer (Carlo-
119 Erba 1110) connected online to a Thermo Finnigan Delta V Plus massspectrometer at the

1
2
3 120 University of Erlangen (Germany). Organic $^{13}\text{C}/^{12}\text{C}$ values are normalized to the international
4
5 121 VPDB standard (Vienna Pee Dee Belemnite). Each sample was analyzed 1 to 4 times;
6
7 122 accuracy and reproducibility of the analyses were checked by replicate analyses of
8
9 123 international standards USGS40 and USGS41. The reproducibility of analyses is within 0.2%
10
11 124 (1σ). The CaCO_3 (%) content of the samples was measured with a Bernard Calcimeter.
12
13
14
15

16 126 **4. Description of lithological units**

17
18 127 Ratschiller (1967) first reported a precise lithology of Cenozoic deposits in Central and
19
20 128 Western Moroccan Sahara, and defined the Izic Formation (Fm.). Ranging from the latest
21
22 129 Miocene up to the Pliocene, the transgressive Aaiun Fm. (Laayoun area) supposed as Late
23
24 130 Miocene in age, and the Paleogene Samlat Fm. Primarily based on foraminifera, Ratschiller
25
26 131 (1967) subdivided the Samlat Fm. in three Members (Mb.) as follows:
27
28

29 132 - the Morcba Mb., which mainly consists of continental sand deposits with some petrified
30
31 133 woods, and that is attributed to the Oligocene.

32
33 134 -Early Miocene despite the lack of age evidence.

34
35 135 - the thick Guerran Mb., which is primarily a marine siliceous chalk, becoming more clastic
36
37 136 farther onshore, and dated to the Eocene on the basis of foraminifera;

38
39 137 -the Itgui Mb., which consists principally of marine limestones with flint levels, dated from
40
41 138 the Paleocene.

42
43 139 The studied deposits of the Dakhla area formally belong to the Samlat Fm., but considering
44
45 140 that the lithology of each Ratschiller's Member was defined further north (near Aauinat
46
47 141 Tartar, south of Boujdour), we decided here to use lithological units without reference to the
48
49 142 Ratschiller's members.

50
51 143 In the Dakhla region, the escarpment lies between 10 and 60m above the sea level, and forms
52
53 144 a west facing cliff, steeping on the upper part but sloping gently at the base. The studied
54
55
56
57
58
59
60

1
2
3 145 sections are directly along a steep cliff at the Atlantic coast exposed between the Gulf of
4
5 146 Cintra and the N'Tireft village (Fig. 1b). The Paleogene formation is overlain by a 1 to 2m
6
7 147 thick lumachellic limestone, which is Mio-Pliocene in age (e.g. Joleaud, 1907, Front Y Sague,
8
9 148 1911, Deperet, 1912, Lecointre, 1966), and consists of:

- 10
11 149 - alternating marine limestones and marls, rich in organic matter at the base;
12
13 150 - alternating sandstones and marls, with intercalations of brown to black siliceous limestones
14
15 151 at the middle interval;
16
17 152 - sandy white marls at the top.
18
19
20
21 153

22 154 **4.a. Garitas section**

23
24
25 155
26
27 156 This section is directly exposed along the cliff located about 15 km north of Imlili village, in a
28
29 157 locality named Garitas, which is located in a restricted military area. Lateral variations of
30
31 158 facies are obvious, especially regarding strata thickness (Fig. 4c). We have divided these
32
33 159 sequences into five lithological units (U1-5).
34
35
36 160

37 38 161 ***Unit U1:***

39
40 162 This unit represents the lowermost part of the section, as in Adnet et al. (2010), and is
41
42 163 composed of a succession of four lithofacies (Fig. 2).
43
44

45 164 1- The first Unit is a rhythmic sequence that consists of gray-beige marl limestone to whitish
46
47 165 surface, sometimes siliceous with splintery fracture. This marly limestone, showing sporadic
48
49 166 black nodules, alternates with marl gray or blackish rich in organic matter (Fig. 3a-c). The
50
51 167 base of this sequence shows a ~10-cm-thick blackish phosphorite with rich organic matter
52
53 168 including numerous coprolites and fish remains (level A1, Fig. 3c). This last level becomes thicker
54
55 169 (20-cm thick) and whiter toward the south.
56
57
58
59
60

1
2
3 170 2- Alternating beige marl and siliceous limestone with vertical fissure filled with the same
4
5 171 sediments (Neptunian dykes; Fig. 3e-f). The limestone beds show inverse graded bedding
6
7 172 (decimetric at the bottom and multi-decimetric at the top). Several coprolite levels (Fig. 4a)
8
9 173 are noted, with centimeter to decimeter thick.

10
11 174 3- Compact gray limestone bars and beige sandy calcareous marl (Fig. 4b).

12
13 175 4- A landmark level composed of black to brown or dark siliceous limestone, rich in
14
15 176 coprolites at its base and alternating with beige marls (Fig. 4b).

16
17
18 177

19
20
21 178 ***Unit U2:***

22
23 179 This second unit is composed of two lithofacies.

24
25 180 5- Yellowish sandy marl ($\approx 1\text{m}$) overlaid by a friable sandy micro-conglomeratic ferruginous
26
27 181 level, which is particularly rich in selachians teeth and vertebrates bones (bed B1 of Adnet et
28
29 182 al., 2010). This fossil-bearing level B1 (Fig. 4c) has yielded a large number of vertebrae of
30
31 183 cetaceans belonging to five different species, with possible rib fragments of sirenians, as well
32
33 184 as few remains of crocodiles, turtles, sea snakes and birds (Zouhri et al., 2014).

34
35 185 6- Whitish marl level with intercalations of lenticular brown siliceous limestone ($\approx 5\text{m}$) (Figs.
36
37 186 4b and 5a).

38
39
40 187

41
42
43 188 ***Unit U3:***

44
45 189 This third unit comprises three lithofacies.

46
47 190 7- Muddy brown yellow sandstone, sometimes with a secondary gypsum element. This level
48
49 191 yields abundant remains of selachians and archaeocetes (basilosaurids) (cf. Bed B2 of Adnet
50
51 192 et al., 2010). Zouhri et al., (2014) reported from this level a *Basilosaurus* sp. and remains of a
52
53 193 dugongid (Fig. 6a, b)

1
2
3 194 8- Fossil-rich beige sandy marl, yielding few dental remains of terrestrial mammals (rodent
4
5 195 **incisor**) and selachians (Level C1).
6

7 196 9- Beige sandy marls.
8
9

10 197
11

12 198 **Unit U4:**

13
14 199 10- Red Sands ($\approx 0.5\text{m}$).
15

16 200 **Unit U5:**

17
18 201 11- A consolidated coquina deposit with oysters and gastropods (scallops bed ($\approx 1,5\text{m}$)).
19
20

21 202
22

23 203 **4.b. Porto Rico section**

24
25 204 The section is located about 10 km east of the Dakhla city, along the seashore of Porto Rico
26
27 205 (Fig. 1b). In this area, the available section starts with the bone-bed fossil-bearing level B1 of
28
29 206 U2 (Fig. 7), the U1 being under water (or perhaps absent?). This section consists from the
30
31 207 bottom to the top of:
32
33

34 208

35
36 209 **Unit U2:**

37
38 210 1- At the seashore edge, the geological section begins with an oxidized sandy marl level, rich
39
40 211 in vertebrate bones and selachian teeth, corresponding to level B1 of Adnet et al. (2010) (Fig.
41
42 212 7a). This very fossiliferous horizon lies on the previous section more than 22m above the sea
43
44 213 level, and plunges northwardly below the sea level.
45
46

47 214 2- Beige to whitish sandy marls topped by a yellowish and oxidized sandy marl level that is
48
49 215 rich in fossils, fossil-bearing level B2 of Adnet et al. (2010) (Fig. 7c). These levels tend to
50
51 216 disappear within a few hundred meters to the north of Porto Rico (see Fig. 11 correlation).
52
53

54 217
55

56 218
57
58
59
60

1
2
3 219 ***Unit U3:***

4
5 220 3- The middle of the section corresponding to the U3 consists of a thick multicolor sandy marl
6
7 221 series, interstratified by sandstone with limestone concretions. A rich level of selachian teeth
8
9 222 and bones (Level C1), was identified in the lower part of this interval (Fig. 7b).

10
11 223

12
13
14 224 ***Unit U4:***

15
16 225 4- This Unit begins with a very characteristic landmark level consisting of gastropod and
17
18 226 oyster coquina (Fig. 7b and 7d), white sandy marls in the middle, with another fossil-bearing
19
20 227 level C2, including sandstone intercalations.

21
22 228

23
24
25 229 ***Unit U5:***

26
27 230 5- The section ends with the Mio-Pliocene flagstone consisting of a coquina limestone, which
28
29 231 includes oyster shells and gastropods (U5).

30
31 232

32
33
34 233 **4.c. North Porto Rico and El Argoub sections**

35
36 234 These two sections are characterized by the development of both U3 and U4 units formed
37
38 235 mainly by sandy marls, and separated by the landmark gastropod coquina limestone (Fig.
39
40 236 8).The U4 shows green marls containing the fossiliferous level C2 at its base, red mudstones
41
42 237 and laminated sandstones in the middle, and white sandy marls at the top. The U5 consists of
43
44 238 a flagstone formed by laminated sandy-limestones containing millimetric grains of quartz.

45
46 239

47
48
49 240 **5. Correlation between the sections**

50
51 241 The North-South logged sections were correlated based on, at least, five remarkable fossil-
52
53 242 bearing levels (noted A1, B1, B2, C1, and C2). In these measured sections, the
54
55 243 aforementioned lithostratigraphic units show lateral variations of facies along the coastline

1
2
3 244 (Fig. 9). These variations can be explained by the slight northward tilting of these deposits.
4
5 245 The five units recognized represent a general regressive trend, which records a transition from
6
7 246 an outer ramp into a peritidal zone. The rhythmic bedding might have been caused by
8
9 247 fluctuations in the depositional environment.
10
11 248 **With the exception of** U5, the four units U1-4 are Paleogene in age and thus formally belong
12
13 249 to the Samlat Fm. (see before). The correlations with the three members of the Samlat Fm. of
14
15 250 Rattschiller (1967) remain hypothetical, and suffer from inconsistent observations.
16
17 251 Rattschiller (1967: fig. 176) illustrated a beach cliff around Porto Rico, where he considered
18
19 252 that the Aaiun Fm. directly overlies the Lebtaina Fm., a formation underlying the Samlat Fm.
20
21 253 However, it seems that what he considered as the Aaiun Fm., rather corresponds to the U3-5
22
23 254 of the Dakhla area, and that the Lebtaina Fm. corresponds to U1-2. Indeed, if it was firstly
24
25 255 expected to attribute the U1-2 to the Guerran Mb. and the U3-4 to the Morcba Mb. According
26
27 256 Rattschiller (1967), we cannot confirm the lithological divisions of Rattchiller (1967).
28
29
30
31
32
33

34 258 **6. Paleomagnetic analysis**

35
36 259
37
38 260 Samples were analyzed with the paleomagnetic facilities housed at the iPHEP of the
39
40 261 Université de Poitiers, France. Remanent magnetization was measured with a JR6
41
42 262 magnetometer combined with stepwise thermal or alternating field demagnetization in a
43
44 263 magnetically shielded room. To better constrain the magnetic mineralogy, we studied the
45
46 264 acquisition of isothermal remanent magnetization (IRM), and then the stepwise thermal
47
48 265 demagnetization of three-axis differential IRM following the method of Lowrie (1990). The
49
50 266 specimens were subjected to stepwise thermal demagnetization in steps up to 600°C. The
51
52 267 IRM was determined with a pulse electromagnet. Thermal demagnetization was done with a
53
54 268 magnetic measurement thermal demagnetizer (MMTD80) shielded furnace. Progressive
55
56
57
58
59
60

1
2
3 269 thermal demagnetization was carried out, in steps of 30 to 40°C, from 100°C, until either the
4
5 270 magnetization intensity fell below the noise level or the direction became erratic. The
6
7 271 majority of specimens were submitted to stepwise alternating field (AF) demagnetization with
8
9 272 increments of 5–10 mT, using a Molspin Ltd. high-field shielded demagnetizer. Characteristic
10
11 273 magnetization components were isolated by applying the method of Kirschvink (1980) to
12
13 274 vector segments with a maximum angular deviation less than 15°.
14
15
16
17

275

276 **6.a. Magnetic properties and characteristic directions**

277

278 A set of rock magnetic experiments was conducted to characterize and identify the magnetic
279 mineralogy of the main lithologies. We first analyzed the acquisition of IRM (Isothermal
280 Remanent Magnetization) up to 500 mT and its subsequent thermal demagnetization.
281 Following the procedure described by Lowrie (1990), magnetic fields of 1, 0.4 and 0.12 T
282 were successively applied to each of the three perpendicular directions prior to thermal
283 demagnetization. The IRM acquisition curves (Fig. 11a) show a broad range of coercivities.
284 The initial increase of magnetization up to 100–150 mT indicates the presence of low
285 coercivity minerals. Saturation was achieved between 300 and 500mT, which indicates the
286 presence of intermediate coercivity minerals.
287 Thermal demagnetization shows that the low field (0.12 T) component is dominant, in figures
288 11b,c, the first drop appears on the soft and medium components between 300°C and 350°C,
289 indicating the existence of magnetic mineral with soft coercivity, probably corresponding to
290 low-Titanomagnetite. The second drop is observed at 580°C indicating the presence of
291 magnetite. The harder components, less than 25% of the total IRM, decrease regularly up to
292 temperature of 300–350°C and suggest the presence of a Fe-sulphide.

1
2
3 293 Thermomagnetic curves are routinely used in paleomagnetism to identify remanence carriers.
4
5 294 Low-field susceptibility measurements (k - T curves) were performed using a Bartington
6
7 295 susceptibility meter (MS-2) equipped with furnace. Some specimens were heated up to 600°C
8
9
10 296 at a heating rate of 10°C·min⁻¹, and then were cooled at the same rate (Fig. 11d). The
11
12 297 thermomagnetic behavior of bulk sediment samples shows very low magnetization, in
13
14 298 agreement with low intensity of the sample. At about 400°C, magnetization starts to increase,
15
16 299 is maximal at about 500°C, and then decreases sharply to 0 just before 600°C. This is due to
17
18 300 the presence of pyrite, a paramagnetic mineral that altered towards magnetite near 500°C
19
20 301 during the experiment (Strechie et al., 2002; Tudryn & Tucholka, 2004). Cooling curves
21
22 302 indicate that magnetite is produced as a result of the thermal breakdown (Fig. 11d). No correct
23
24 303 curve was obtained for the majority of samples because of low initial signal of magnetic
25
26 304 susceptibility.

27
28
29
30 305 The natural remanent magnetization displays moderately high values, starting at 8.8×10^{-7} A/m
31
32 306 in siltstone levels, and reaching up to $\sim 6.3 \times 10^{-4}$, with an average of 1.9×10^{-4} A/m (Fig. 10).
33
34 307 After some step demagnetization, the magnetization intensity fell below noise level of the
35
36 308 magnetometer (Fig. 12a), and the direction became erratic (Fig. 12b). Data resulting from AF
37
38 309 and thermal demagnetization were plotted on orthogonal vector plots (Zijderveld, 1967). To
39
40 310 determine characteristic magnetic directions, principal components analysis was carried out
41
42 311 on all samples. These paleomagnetic directions were then analyzed, using Fisher statistics, to
43
44 312 determine site mean declinations, mean inclinations and associated precision parameters.
45
46 313 Only tree strata at the upper part of the section gives a coherent result of normal direction
47
48 314 (Fig. 12c). The mean directions of ChRM are: declination = 324.4°, inclination = 44.6° (α_{95}
49
50 =24.4, $k = 6$), and differ from the expected direction for this latitude ($I=27.2$, $D=352.2$) (Fig.
51
52 315 12d).
53
54 316
55
56
57
58
59
60

318 7. Carbon isotope geochemistry results

319 Carbon isotopic values range from -27.8‰ (sample ARG15-2) to -22.1‰ (sample PTO15-11;
320 Table 1). These data are in good agreement with the expected $\delta^{13}\text{C}$ values on organics at the
321 Eocene-Oligocene interval (see Sarkar et al., 2003). Seven samples have Total Organic
322 Carbon too low (<0.01%) to perform reliable isotopic analysis.

323 In the Porto-Rico section, the $\delta^{13}\text{C}_{\text{org}}$ curve shows the following successive
324 values/trends, from the base to the top (Fig. 13; Table 1):

- 325 1. relatively negative $\delta^{13}\text{C}_{\text{org}}$ value (-27.6‰) in the B1 fossil-bearing level, at the base of
326 the section (lowermost part of unit U2);
- 327 2. relatively stable $\delta^{13}\text{C}_{\text{org}}$ values (from -25.1 to -24.3‰) in the U2 (including the fossil-
328 bearing B2 level);
- 329 3. relatively negative $\delta^{13}\text{C}_{\text{org}}$ value, around -25.7‰ in the lower part of U3 (including the
330 C1 fossil-bearing level);
- 331 4. relatively stable $\delta^{13}\text{C}_{\text{org}}$ values (from -25.2 to -24.6‰) in the upper part of U3;
- 332 5. prominent and rapid positive shift of $\delta^{13}\text{C}_{\text{org}}$ values, from -26.2‰ to -22.1‰ in the
333 uppermost part of U3 and U4;
- 334 6. negative shift of $\delta^{13}\text{C}_{\text{org}}$ values, from -22.1‰ to -25.4‰ in the lower part of U5
335 (including the C2 fossil-bearing level);
- 336 7. positive shift of $\delta^{13}\text{C}_{\text{org}}$ values, from -25.4‰ to -23.7‰ in the upper part of U5;
- 337 8. negative shift of $\delta^{13}\text{C}_{\text{org}}$ values, from -23.7‰ to -25.2‰ in the uppermost part of U5.

338 In the El Argoub section, the $\delta^{13}\text{C}_{\text{org}}$ curve shows the following successive values/trends, from
339 the base to the top (Fig. 13; Table 1):

- 340 1. prominent and rapid positive shift of $\delta^{13}\text{C}_{\text{org}}$ values, from -27.8‰ to -23.4‰ in the
341 uppermost part of U3 and U4;

- 1
2
3 342 2. negative shift of $\delta^{13}\text{C}_{\text{org}}$ values, from -23.4‰ to -25.7‰ in the lower part of U5
4
5 343 (including the C2 fossil-bearing level);
6
7 344 3. positive shift of $\delta^{13}\text{C}_{\text{org}}$ values, from -25.7‰ to -23.0‰ in the upper part of U5;
8
9 345 4. negative shift of $\delta^{13}\text{C}_{\text{org}}$ values, from -23.0‰ to -25.5‰ in the uppermost part of U5.

11 346 The CaCO_3 contents range from 0.0 to 76.9% in the Porto-Rico section and from 0.0 to 45.3%
12
13 347 in the El Argoub section.

14
15
16 348

18 349 **8- DISCUSSION**

19 350

21 351 The fossil content of the Dakhla deposits is rich and varied, mixing primarily selachians and
22
23 352 marine mammals (cetaceans and sirenians). Ratschiller (1967) first mentioned the occurrence
24
25 353 of fish teeth in the Eocene Guerran Mb. of the Samlat Fm. In the Dakhla area, a rich
26
27 354 vertebrate fauna was discovered by Adnet et al., (2010) in two levels: B1 and B2. The Eocene
28
29 355 age proposed by Ratschiller (1967) and later by Adnet et al. (2010) was based on
30
31 356 paleontological evidence. Indeed, the majority of selachian taxa (such as *Xiphodolamia*
32
33 357 *serrata*, *Misrichthys stromeri* and *Cretolamna twiggsensis*) recovered in B1 and B2 are
34
35 358 known elsewhere in deposits dating from the Bartonian and Priabonian (e.g. Qasr El Sagha
36
37 359 Fm. [Egypt], Qa'Faydat and the Wadi Esh-Shallala Fm. [Jordan], or the Drazinda Shale Mb.
38
39 360 of the Kirthar Fm. [Pakistan] (Adnet et al., 2010). Later, Zouhri et al. (2014) described five
40
41 361 archaeocete cetacean species from the level B1, and dugongid sirenians in the level B2; faunal
42
43 362 correlations with the late Eocene of Egypt indicate a Priabonian age for the B1 and B2 fossil
44
45 363 assemblages.

47
48
49 364 Since 2013, our fieldwork allowed the discovery of new fossil-bearing levels in the
50
51 365 stratigraphic sequence (A1, C1, and C2). The lowermost part of the Garitas section (U1; Figs.
52
53 366 2 and 3) has yielded a fossil-bearing level including a diverse assemblage of fish (e.g.
54
55 367 "*Carcharias*" *koerti*, *Physogaleus* aff. *tertius*, *Coupatzia* spp. *Merabatis* sp., *Burhnamia* sp.,
56
57
58
59
60

1
2
3 368 *Cyladrincanthus* sp.). In the Porto Rico section (Fig. 7), two stratigraphically distinct levels
4
5 369 have yielded fossil vertebrates. The level C1, located at the base of U3 has yielded an
6
7 370 assemblage of selachians (e.g. *Carcharhinus* spp. *Carcharias* sp., *Pristis* cf. *lathamii*,
8
9 371 *Pastinachus* sp., *Aetobatis* cf. *irregularis*). Above in the section, the base of U4 has yielded a
10
11 372 fossil assemblage (C2) of marine and estuarine invertebrates (lamellibranches) and vertebrates
12
13 373 (including fishes, turtles, crocodiles, and selachians resembling to C1), together with
14
15 374 terrestrial mammals (including rodents, primates, hyracoids, an elephant shrew, and
16
17 375 creodonts). A strictly similar fossil assemblage was found in the El Argoub section, in
18
19 376 equivalent deposits (i.e. at the base of U4).

20
21
22
23 377 The mammal fossils of C2 (Porto Rico and El Argoub) consist of isolated teeth, but also
24
25 378 partial jaws and bone fragments. Among the mammals, afrotherians are illustrated by a
26
27 379 herodotiine macroscelid (*Herodotius* aff. *pattersoni*) and several “sagatheriid” hyracoids,
28
29 380 among which is a species of *Sagatherium*. Primates include an oligopithecoid anthropoid
30
31 381 (*Catopithecus* aff. *browni*) and an indeterminate afrotarsiid. Rodents are much more abundant
32
33 382 and represented by members of two phylogenetically distinct groups: Hystricognathi and
34
35 383 Anomaluroidea. Several tens of isolated teeth of anomaluroids indicate the presence of two
36
37 384 distinct families, Anomaluridae and Nonanomaluridae, and possibly the ancestral family
38
39 385 Zegdomyidae, represented by five new species (*Argouburus minutus*, *Paranomalurus*
40
41 386 *riodeoroensis*, *Dakhlamys ultimus*, *Oromys zenkerellinopsis*, and *Nonanomalurus parvus*; see
42
43 387 Marivaux et al. 2017). Regarding hystricognaths (Marivaux et al., in press), distinct taxa are
44
45 388 recognized, primarily including several “phiomyid”-like representatives (*Birkamys* aff. *korai*,
46
47 389 *Mubhammys* sp. nov., *?Phiocricetomys* sp., *Neophiomys* sp. nov., and a new genus and
48
49 390 species) and gaudeamurids (*Gaudeamus* cf. *hylaeus* and *G.* cf. *aslius*). Most of these Dakhla
50
51 391 C2 mammals (except anomaluroids; Marivaux et al., 2017), or at least their close relatives,
52
53 392 have been originally described from well-known Egyptian localities of the Jebel Qatrani
54
55
56
57
58
59
60

1
2
3 393 Formation (Fayum Depression), dating from the latest Eocene (L-41; Hyracoidea: Rasmussen
4
5 394 & Gutiérrez 2010; Macroscelididae: Simons et al. 1991; Primates: Simons 1995; Simons &
6
7 395 Rasmussen 1996; Seiffert 2012; Rodentia: Sallam et al. 2011; Sallam & Seiffert, 2016) or the
8
9 396 early Oligocene (Hyracoidea: Rasmussen & Gutiérrez 2010; Rodentia: Wood, 1968). This
10
11 397 faunal similarity thus indicates a latest Eocene-early Oligocene time frame for the
12
13 398 fossiliferous concentration of the level C2 of the Pto-Arg sector.

14
15
16 399 Here we performed new chemostratigraphic investigation using carbon isotopes from
17
18 400 dispersed organic matter ($\delta^{13}\text{C}_{\text{org}}$) on the Porto Rico and El Argoub sections, in order to refine
19
20 401 the stratigraphic framework of the Samlat Fm. in the Dakhla area. As mentioned above, Adnet
21
22 402 et al. (2010) suggested a Bartonian to Priabonian age for the fossil-bearing levels B1 and B2
23
24 403 on the basis of the selachian fauna. Later, Zouhri et al. (2014) refined the age of the level B1
25
26 404 and proposed early-middle Priabonian on the basis of the cetacean fauna. These authors also
27
28 405 suggested a Priabonian age for the level B2 on the basis of the sirenian fauna. It implies that
29
30 406 the lower part of the studied sections, containing the levels B1 and B2, is (early-middle)
31
32 407 Priabonian in age, thereby suggesting that the upper part of the section is Priabonian or
33
34 408 younger.

35
36
37
38 409 The Eocene–Oligocene boundary (EOB; ~ 34Ma) is the largest global cooling of the
39
40 410 Cenozoic Era and led the Earth's climatic system to change from a greenhouse to an icehouse
41
42 411 mode, well documented in marine setting (e.g. Bohaty et al., 2012) and, to a lesser extent in
43
44 412 continental setting (e.g. Tramoy et al., 2016). The cooling interval, initiated in the late
45
46 413 Eocene, comprise several isotopic events, which have been coded by Miller et al. (1991). The
47
48 414 oldest of the events, coded Oi-1 or Eocene-Oligocene (climate) transition or EOT, is
49
50 415 associated with major $\delta^{18}\text{O}$ and $\delta^{13}\text{C}$ positive shifts, starting in the late Eocene and ending in
51
52 416 the early Oligocene (e.g. Coxall et al., 2005; Katz et al., 2008; Lear et al., 2008). Using a
53
54 417 high-resolution carbon isotope study of the ODP site 1218, Erhardt et al. (2013) showed that
55
56
57
58
59
60

1
2
3 418 the carbon and oxygen positive shifts of the Oi-1 event are followed by two positive $\delta^{13}\text{C}$ and
4
5 419 $\delta^{18}\text{O}$ excursions called Oi-1a and Oi-1b, early Oligocene in age. This isotopic pattern was also
6
7 420 observed by Zhifei et al. (2004) in ODP Leg 208 Site 1262, 1265 and 522.
8

9
10 421 In the Porto Rico (Pto) and El Argoub (Arg) sections (this study; Fig.13), the Oi-1 event
11
12 422 initiates in the uppermost part of the U3 lithological unit (~ 2 meters below the C2 level) and
13
14 423 ends below the C2 level. This isotopic event is followed by one positive excursion (positive
15
16 424 shift followed by a negative shift), interpreted here as Oi-1a. In summary, the C2 level is
17
18 425 clearly above the Oi-1, and as such it is **probably** earliest Oligocene in age.
19

20
21 426 Lower, the B1 and B2 fossil-bearing levels are dated **as** Priabonian by the selachian, cetacean
22
23 427 and sirenian faunas (see above). The C1 level is located in a negative $\delta^{13}\text{C}$ excursion (Fig.13).
24
25 428 This latter should correspond to the carbon isotope excursion observed in the Priabonian
26
27 429 (NP19-20 Zones). The B1 level shows negative $\delta^{13}\text{C}$ value, most probably corresponding to
28
29 430 the negative $\delta^{13}\text{C}$ values in the early Priabonian NP18 Zone (Fig.13).
30

31
32 431 The paleomagnetic analysis show that the only normal polarity is represented by tree strata
33
34 432 situated 2m above the C1 fossiliferous level. Although the rock magnetic properties suggest
35
36 433 that the NRM may be of primary origin, we evaluate other criteria to infer the origin of the
37
38 434 observed characteristic remanence. In situ site mean directions differ significantly from the
39
40 435 direction of the axial geocentric dipole at the latitude of the site (Fig. 12D) and, therefore,
41
42 436 exclude a recent magnetic overprint. Correlation of the Porto Rico section with the
43
44 437 geomagnetic polarity time scale (GPTS) of Gradstein et al. (2012) was performed by
45
46 438 considering the earliest Oligocene age discussed above for C2 level and Priabonian age for B2
47
48 439 and C1. Taking into account the biochronological age, the normal polarity might then be
49
50 440 correlated to ChronC16n.
51

52
53
54 441
55
56
57
58
59
60

1
2
3 442 Our new chemostratigraphic and paleomagnetic data suggest that the C2 fossil-bearing level
4
5 443 of Dakhla is clearly located above the Oi-1 event and below the Oi-1a event. The Oi-1 event,
6
7 444 bringing the major cooling, is recognized by many authors to occur a few 100 kyr later than
8
9 445 the GSSP (Global Boundary Stratotype Section and Point) of the Rupelian (Eocene-Oligocene
10
11 446 boundary; Vandenberghe et al., 2012). The GSSP of the Eocene-Oligocene boundary is
12
13 447 defined in the Massignano section (Italy), and the key marker of the GSSP is the extinction of
14
15 448 the hantkeninid planktonic foraminifera, which lies within nannofossil Zone NP21 (Premoli-
16
17 449 Silva & Jenkins, 1993). Katz et al. (2008) showed that 1) the Oi-1 event is located around the
18
19 450 transition of Chron C13r and C13n (33.545 Myr), and 2) the Oi-1a event is located around the
20
21 451 transition of Chron C13n and C12r. It suggests that the C2 level, located just above the Oi-1
22
23 452 event and below the Oi-1a event, is a few 100 kyr above the Eocene-Oligocene boundary,
24
25 453 within the nannofossil Zone NP21 and into the magnetic polarity Chron 13n. Interestingly, as
26
27 454 mentioned above, Gingerich (1993) suggested that the L-41 level (lower part of the Jbel
28
29 455 Qatrani Fm.) is located in the early Oligocene. Underwood et al. (2013) places the base of the
30
31 456 Jebel Qatrani Formation close to the base of Chron C13n. On the other hand, Seiffert (2006)
32
33 457 concluded that the L-41 of Fayum bed falls within a zone of reverse polarity and correlated
34
35 458 with Chron 13r, late Eocene, i.e. older than the C2 level of Dakhla. The new rodent
36
37 459 assemblage from the earliest Oligocene of Dakhla (Sahara, Morocco), represents therefore the
38
39 460 first Oligocene record of rodents from northwestern Saharan Africa, especially from the
40
41 461 Atlantic margin of that landmass. The carbon isotope chemostratigraphy confirms that the
42
43 462 lower part of the studied sections, containing the levels B1 and B2, is early-middle Priabonian
44
45 463 in age.

51
52 464 Our knowledge of the mammal faunas documenting the early Oligocene of Afro-Arabia has
53
54 465 so far derived from contemporary localities found in northern Egypt (Fayum Depression),
55
56 466 Libya (Zallah Oasis) and Oman (Dhofar Province) (Fejfar, 1987; Sallam et al., 2011, 2016,
57
58
59
60

1
2
3 467 Coster et al., 2010, 2012, Sallam & Seiffert, 2016). This new earliest Oligocene mammal
4
5 468 fauna from the northern Atlantic margin of Africa is of great interest because it documents for
6
7 469 the first time the diversity of micomammals, especially rodents. **Biochronology and C isotope**
8
9 470 **chemostratigraphy provide an Oligocene age constraint of C2 fossiliferous level, and thus**
10
11 471 **increase our understanding of the timing of mammal evolution and environmental changes in**
12
13 472 **North Africa at that time.**

16 473 **Acknowledgments**

17
18
19 474 We would like to thank Abdallah Tarmidi and Mbarek Fouadasi for their help during the field
20
21 475 work. Financial supports during the field work were provided by the French ANR EVAH
22
23 476 (ANR-09-BLAN-0238) and ANR-ERC PALASIAFRICA (ANR-08-JCJC-0017) Programs,
24
25 477 the ISE-M UMR 5554CNRS/UM/IRD/EPHE, CNRS-CoopIntEER171834, and iPHEP UMR
26
27 478 CNRS 7262. C.N. and J.Y thank the project BR/121/A3/PALEURAFRICA of the Belgian Science
28
29 479 Policy Office.
30
31
32

33 480
34
35
36
37
38
39
40
41
42
43
44
45
46
47
48
49
50
51
52
53
54
55
56
57
58
59
60

481 **REFERENCES CITED**

- 482 ADNET, S., CAPPETTA, H. & TABUCE, R. 2010. A Middle–Late Eocene vertebrate fauna
483 (marine fish and mammals) from southwestern Morocco; preliminary report: age and
484 palaeobiogeographical implications. *Geological Magazine* **147**, 860–870.
- 485 BENAMMI, M., ELKATI, I., ADNET, S., MARIVAUX, L., TABUCE, R., SURAULT, J.,
486 BAIDDER, L., SADDIQUI, O. & BENAMMI, M. 2014. Corrélation de coupes
487 lithostratigraphiques le long des falaises côtières dans la région d’El Argoub (Dakhla,
488 Maroc): Second North African Vertebrate Palaeontology Congress-NAVEP2,
489 Ouarzazate, Morocco, 1-8 September, Abstracts, p.37.
- 490 BENAMMI, M., ELKATI, I., ADNET, S., MARIVAUX, L., TABUCE, R., SURAULT, J.,
491 BAIDDER, L., SADDIQUI, O. & BENAMMI, M., 2014. Preliminary paleomagnetic data
492 in the Dakhla, Southwestern Moroccan Sahara: Second North African Vertebrate
493 Palaeontology Congress-NAVEP2, Ouarzazate, Morocco, 1-8 September, Abstracts,
494 p.40.
- 495 BOHATY, S.M., ZACHOS, J.C. & DELANEY, M.L. 2012. Foraminiferal Mg/Ca evidence
496 for Southern Ocean cooling across the Eocene/Oligocene transition. *Earth and*
497 *Planetary Science Letters* **317–318**, 251–261.
- 498 COSTER, P., BENAMMI, M., LAZZARI, V., BILLET, G., MARTIN, T., SALEM, M.,
499 ABOLHASSAN BILAL, A., CHAIMANEE, Y., SCHUSTER, M., VALENTIN, X.,
500 BRUNET, M. & JAEGER, J.-J., 2010. *Gaudeamuslavocati* sp. nov. (Rodentia,
501 Hystricognathi) from the lower Oligocene of Zallah, Libya: First African Caviomorph?.
502 *Naturwissenschaften* **97**, 697-70.
- 503 COSTER, P., BENAMMI, M., SALEM, M., BILAL AWAD, A., CHAIMANEE, Y.,
504 VALENTIN, X., BRUNET M. & JAEGER, J.J., 2012. New hystricognathous rodent
505 from the Early Oligocene of central Libya, (Zallah Oasis, Sahara Desert): systematic,

- 1
2
3 506 phylogenetic, and biochronologic implications. *Annals of Carnegie Museum* **80**, 239–
4
5 507 259.
6
7 508 COXALL, H.K., WILSON, P.A., PÄLIKE, H., LEAR, C.H. & BACKMAN, J. 2005. Rapid
8
9 509 stepwise onset of Antarctic glaciation and deeper calcite compensation in the Pacific
10
11 510 Ocean. *Nature* **433**, 53–57.
12
13 511 CRAMER, B.S., TOGGWEILER, J.R., WRIGHT, J.D., KATZ, M.E. & MILLER, K.G.,
14
15 512 2009. Ocean overturning since the Late Cretaceous: inferences from a new benthic
16
17 513 foraminiferal isotope compilation. *Paleoceanography*, published online 23 December
18
19 514 2009.doi:10.1029/2008PA001683.
20
21 515 DAVISON, I. 2005. Central Atlantic margin basins of North West Africa: geology and
22
23 516 hydrocarbon potential (Morocco to Guinea). *Journal of African Earth Sciences* **43** (1-3),
24
25 517 254–274.
26
27 518 DAVISON, I. & DAILLY, P. 2010. Salt tectonics in the Cap Boujdour Area, Aaiun Basin,
28
29 519 NW Africa. *Marine and Petroleum Geology* **27**, 435–441.
30
31 520 DEPERET, C. 1912. Sur l'âge des couches du Rio de Oro. *Comptes Rendus de l'Académie*
32
33 521 *des Sciences* **13**, 123-124
34
35 522 ERHARDT, A.M., PÄLIKE H. & PAYTAN. A. 2013. High-resolution record of export
36
37 523 production in the eastern equatorial Pacific across the Eocene-Oligocene transition and
38
39 524 relationships to global climatic records. *Paleoceanography*, published online 25 March
40
41 525 2013.doi:10.1029/2012PA002347.
42
43 526 FEJFAR, O. 1987. Oligocene rodents from Zallah Oasis, Libya. *Münchner*
44
45 527 *Geowissenschaftliche Abhandlungen* A10, 265–268.
46
47 528 FRONT Y SAGUE, N. 1911. Les formations géologiques du Rio de Oro, Sahara espagnol.
48
49 529 *Bulletin de la Société Géologique de France* **4**, 212-217
50
51
52
53
54
55
56
57
58
59
60

- 1
2
3 530 JOLEAUD, L. 1907. Note sur quelques dents de Poissons fossiles du Rio de Oro (Sahara
4
5 531 occidental). *Bulletin de la Société Géologique de France* **7**, 514.
6
7 532 GINGERICH, P.H. 1993. Oligocene age of the Gebel Qatrani Formation, Fayum, Egypt.
8
9 533 *Journal of Human Evolution* **24**, p. 207-218.
10
11 534 GRADSTEIN, F.M., OGG, J.G., SCHMITZ, M.D., & OGG, G.M., (eds.), 2012. The geologic
12
13 535 time scale 2012. Amsterdam, Netherlands, Elsevier, 1144 p.
14
15
16 536 KATZ, M.E., MILLER, K.G., WRIGHT, J.D., WADE, B.S., BROWNING, J.V., CRAMER,
17
18 537 B.S. & ROSENTHAL, Y. 2008. Stepwise transition from the Eocene greenhouse to the
19
20 538 Oligocene icehouse. *Nature Geosciences* **1**, 329–334.
21
22
23 539 KIRSCHVINK, J.L. 1980. The least-square line and plane and analysis of palaeomagnetic
24
25 540 data. *Geophysical Journal of the Royal Astronomical Society* **62**, 699-718.
26
27 541 KLINGELHOEFER, F., LABAILS, C., COSQUER, E., ROUZO, S., GÉLI, L., ASLANIAN,
28
29 542 D., OLIVET, J.-L. , SAHABI, M., NOUZÉ, H. & UNTERNEHR, P. 2009. Crustal
30
31 543 structure of the SW-Moroccan margin from wide-angle and reflection seismic data (the
32
33 544 Dakhla experiment) Part A: Wide-angle seismic models. *Tectonophysics* **468**, p. 63–82.
34
35
36 545 KOLONIC, S., SINNINGHEDAMSTÉ, J.S., BÖTTCHER, M.E., KUYPERS, M.M.M.,
37
38 546 KUHNT, W., BECKMANN, B., SCHEEDER, G. & WAGNER, T. 2002. Geochemical
39
40 547 characterization of Cenomanian/Turonian black shales from the Tarfaya Basin (SW
41
42 548 Morocco). *Journal of Petroleum Geology* **25**, 325-350.
43
44
45 549 LEAR, C.H., BAILEY, T.R., PEARSON, P.N., COXALL, H.K. & ROSENTHAL, Y. 2008.
46
47 550 Cooling and ice growth across the Eocene-Oligocene transition. *Geology* **36**, 251–254.
48
49 551 LECOINTRE, G. 1962. Sur la géologie de la presqu'île de villa Cisneron, Rio de Oro.
50
51 552 *Comptes Rendus de l'Académie des Sciences* **254**, 1121-1122.
52
53
54 553 LECOINTRE, G. 1966. Néogène et Quaternaire du Rio de Oro (Maroc Espagnol). *Comptes*
55
56 554 *Rendus de l'Académie des Sciences* **10**, 404-405.
57
58
59
60

- 1
2
3 555 LIU, Z., TUO, S., ZHAO, Q., CHENG, X. & HUANG, W. 2004. Deep-water earliest
4
5 556 Oligocene Glacial Maximum (EOGM) in South Atlantic. *Chinese Science Bulletin* **49**,
6
7 557 2190-2197.
8
9
10 558 LOWRIE, W. 1990. Identification of ferrimagnetic minerals in rock by coercivity and
11
12 559 unblocking temperature properties. *Geophysical Research Letters*, **17**, 159–162.
13
14 560 MARIVAUX, L., ADNET, S., BENAMMI, M., TABUCE, R., & BENAMMI, M., 2017.
15
16 561 Anomaluroid rodents from the earliest Oligocene of Dakhla, Morocco, reveal the long-
17
18 562 lived and morphologically conservative pattern of the Anomaluridae and
19
20 563 Nonanomaluridae during the Tertiary in Africa. *Journal of Systematic Palaeontology*,
21
22 564 published online 10 August 2016, doi:10.1080/14772019.2016.1206977.
23
24
25 565 MARIVAUX, L., ADNET, S., BENAMMI, M., TABUCE, R., YANS, Y., & BENAMMI,
26
27 566 M., in press. Earliest Oligocene hystricognathous rodents from the Atlantic margin of
28
29 567 Northwestern Saharan Africa (Dakhla, Morocco): systematic, paleobiogeographical and
30
31 568 paleoenvironmental implications. *Journal of Vertebrate Paleontology*.
32
33
34 569 MILLER, K.G., WRIGHT, J.D. & FAIRBANKS, R.G. 1991. Unlocking the ice house:
35
36 570 Oligocene-Miocene oxygen isotopes, eustasy and margin erosion. *Journal of*
37
38 571 *Geophysical Research* **96**, 6829-6848.
39
40
41 572 ORTLIEB, L. 1975. Recherches sur les formations plio-quaternaire du littoral Ouest Saharien
42
43 573 (28°30'-20°40'). PhD thesis, Pierre et Marie-Curie University, Paris VI - Trav. et Doc.
44
45 574 ORSTOM, **48**, 267p.
46
47 575 PREMOLI-SILVA, I. & JENKINS, D.G. 1993. Decision on the Eocene-Oligocene boundary
48
49 576 stratotype. *Episodes* **16**, 379-382.
50
51
52 577 RANKE, U., VON RAAD, U. & WISSMANN, G. 1982. Stratigraphy, facies, and tectonic
53
54 578 development of on- and offshore Aaiun-Tarfaya Basin a review. In *Geology of the*
55
56 579 *North West African Continental Margin* (ed U. Von Raad), pp 86–104. Springer-Verlag.

- 1
2
3 580 RASMUSSEN, D.T. & GUTIÉRREZ, M. 2010. Hyracoidea. In the Cenozoic Mammals of
4
5 581 Africa (eds L.Werdlin & W.J. Sanders), pp.123-146. University of California Press,
6
7 582 Berkeley.
- 8
9 583 RATSCHILLER, L.K. 1967. Sahara, correlazioni geologico-litostratigrafiche fra Sahara
10
11 584 Centrale ed Occidentale. *Mem. Mus. Tridentino Sc. Nat.*, **16**, 55-190.
- 12
13 585 RJIMATI, E., ZEMMOURI, A., BENLAKHDIM, A., AMZAEHOU, M., ESSALMANI, B.,
14
15 586 MUSTAPHI, H., HAIMOUK, M. & HAMIDI, F. 2008. Carte Géologique du Maroc.
16
17 587 Ad-Dakhla, 1/100 000. *Notes et Mémoires Service Géologique du Maroc*, 487
- 18
19 588 SADDIQI, O., RJIMATI, E., MICHARD, A., SOULAIMANI, A. & OUANAIMI, H. 2015.
20
21 589 Recommended Geoheritage Trails in Southern Morocco: A 3 Ga Record Between the
22
23 590 Sahara Desert and the Atlantic Ocean. In *From Geoheritage to Geoparks, Case Studies*
24
25 591 *from Africa and Beyond* (eds E. Errami, B. Margaret & S. Vic), pp. 91-108. Springer.
- 26
27 592 SACHSE, V.F., LITCKE, R., HEIM, S., KLUTH, O., SCHOBER, J., BOUTIB, L., JABOUR,
28
29 593 H., PERSSSEN, F. & SINDERN, S., 2011. Petroleum source rocks of the Tarfaya Basin
30
31 594 and adjacent areas, Morocco. *Organic Geochemistry* **42**, 209-227.
- 32
33 595 SACHSE, V.F., HEIM, S., JABOUR, H., KLUTH, O., SCHÜMANN, T., AQUIT, M. &
34
35 596 LITCKE, R. 2014. Organic geochemical characterization of Santonian to Early
36
37 597 Campanian organic matter-rich marls (Sondage No. 1 cores) as related to OAE3 from
38
39 598 the Tarfaya Basin, Morocco. *Marine and Petroleum Geology* **56**, 290-304.
- 40
41 599 SALLAM, H.M., SEIFFERT, E.R. & SIMONS, E.L. 2011. Craniodental morphology and
42
43 600 systematics of a new family of hystricognathous rodents (Gaudeamuridae) from the
44
45 601 Late Eocene and Early Oligocene of Egypt. *PLoS ONE* **6**, e16525eol.
- 46
47 602 SALLAM, H.M. & SEIFFERT, E.R. 2016. New phiomorph rodents from the latest Eocene of
48
49 603 Egypt, and the impact of Bayesian “clock” based phylogenetic methods on estimates of
50
51 604 basal hystricognath relationships and biochronology. *PeerJ* **4**, e1717.
- 52
53
54
55
56
57
58
59
60

- 1
2
3 605 SARKAR, A., SARANGIB, S., EBIHARAC, M., BHATTACHARYAD, S.K. & RAYE,
4
5 606 A.K. 2003. Carbonate geochemistry across the Eocene/Oligocene boundary of Kutch,
6
7 607 western India: implications to oceanic O₂-poor condition and foraminiferal extinction:
8
9 608 *Chemical Geology* **201**, 281–293.
- 10
11 609 SEIFFERT, E.R. 2006. Revised age estimates for the later Paleogene mammal faunas of
12
13 610 Egypt and Oman. *Proceedings of the National Academy of Sciences of the USA* **103**,
14
15 611 5000–5005.
- 16
17 612 SEIFFERT, E.R. 2012. Early primate evolution in Afro-Arabia. *Evolutionary Anthropology*
18
19 613 **21**, 239–253.
- 20
21 614 SIMONS, E.L. & RASMUSSEN, D.T. 1996. Skull of *Catopithecus browni*, an early Tertiary
22
23 615 catarrhine. *American Journal of Physical Anthropology* **100**, 261–292.
- 24
25 616 SIMONS, E.L., HOLROYD, P.A & BOWN, T.M. 1991. Early Tertiary elephant shrews from
26
27 617 Egypt and the origin of the Macroscelidea. *Proceedings of the National Academy of*
28
29 618 *Sciences of the USA* **88**, 9734–9737.
- 30
31 619 STORME, J.-Y., DEVLEESCHOUWER, X., SCHNYDER, J., CAMBIER, G., BACETA,
32
33 620 J.I., PUJALTE, V., IACUMIN, P. & YANS, J. 2012. Paleocene/Eocene boundary
34
35 621 section at Zumaia (Basque-Catatic Basin) revisited: new insights from high resolution
36
37 622 magnetic susceptibility and carbon isotope chemostratigraphy on organic matter
38
39 623 ($\delta^{13}\text{C}_{\text{org}}$). *Terra Nova* **24**, 310–317.
- 40
41 624 STRECHIE, C., ANDRE, F., JELINOWSKA, A., TUCHOLKA, P., GUICHARD, F.,
42
43 625 LERICOLAIS, G. & PANIN, N. 2002. Magnetic minerals as indicators of major
44
45 626 environmental change in Holocene Black Sea sediments: preliminary results. *Physics*
46
47 627 *Chemistry Earth* **27**, 1363–1370.
- 48
49 628 TRAMOY, R., SALPIN, M., SCHNYDER, J., PERSON, A., SEBILO, M., YANS, J.,
50
51 629 VAURY, V., FOZZANI, J. & BAUER, H. 2016. Stepwise paleoclimate change across
52
53
54
55
56
57
58
59
60

- 1
2
3 630 the Eocene-Oligocene transition recorded in continental NW Europe by mineralogical
4
5 631 assemblages and $\delta^{15}\text{N}_{\text{org}}$ (Rennes Basin, France). *Terra Nova* **28**, 212–220
6
7 632 TUDRYN, A. & TUCHOLKA, P. 2004. Magnetic monitoring of thermal alteration for natural
8
9 633 pyrite and greigite. *Acta Geophysica Polonica* **52**, 509–520.
10
11 634 UNDERWOOD, C.J., KING, C. & STEURBAUT, E. 2013. Eocene initiation of Nile
12
13 635 drainage due to East African uplift. *Palaeogeography, Palaeoclimatology,*
14
15 636 *Palaeoecology* **392**, 138–145.
16
17 637 VANDENBERGHE, N., HILGEN, F.J. & SPEIJER, R. 2012. The Paleogene Period. In *The*
18
19 638 *Geological Time Scale*. (eds F.M. Gradstein, J.G. Ogg, M.D. Schmitz, G.M. Ogg).
20
21 639 2012. Elsevier Science Ltd, Oxford **2**, 855-921.
22
23 640 YANS, J., GERARDS, T., GERRIENNE, P., SPAGNA, P., DEJAX, J., SCHNYDER, J.,
24
25 641 STORME, J.-Y. & KEPPENS, E. 2010. Carbon-isotope of fossil wood and dispersed
26
27 642 organic matter from the terrestrial Wealden facies of Hautrage (Mons basin, Belgium).
28
29 643 *Palaeogeography, Palaeoclimatology, Palaeoecology* **291**, 85-105.
30
31 644 WOOD, A.E. 1968. Part II: The African Oligocene Rodentia; in *Early Cenozoic Mammalian*
32
33 645 *Faunas Fayum Province, Egypt* (ed J.E. Remington). pp. 23–105. Peabody Museum of
34
35 646 Natural History Yale University, New Haven, Connecticut.
36
37 647 ZHIFEI, L., SHOUTING, T., QUANHONG Z., XINRONG, C. & WEI, H. 2004. Deep-water
38
39 648 Earliest Oligocene Glacial Maximum (EOGM) in South Atlantic. *Chinese Science*
40
41 649 *Bulletin* **49**, 2190-2197.
42
43 650 ZIJDERVELD, J. D. A. 1967. AC demagnetization rocks-Analyses of results. In *Methods in*
44
45 651 *paleomagnetism* (eds D. W. Collinson, K.M. Creer & S.K. Runcorn), p. 254–286.
46
47 652 Amsterdam, Netherlands, Elsevier Scientific.
48
49 653 ZOUHRI, S., GINGERICH, P.D., EL BOUDALI, N., SEBTI, S., NOUBHANI, A., RAHALI,
50
51 654 M. & MESLOUH, S. 2014. New marine mammal faunas (Cetacea and Sirenia) and sea
52
53
54
55
56
57
58
59
60

1
2
3 655 level change in the Samlat Formation, upper Eocene, near Ad-Dakhla in southwestern
4
5 656 Morocco. *Comptes Rendus Palevol* **13**, 599-610.
6

7 657
8

9 658
10
11
12
13
14
15
16
17
18
19
20
21
22
23
24
25
26
27
28
29
30
31
32
33
34
35
36
37
38
39
40
41
42
43
44
45
46
47
48
49
50
51
52
53
54
55
56
57
58
59
60

Proof For Review

1
2
3 **659 Figures captions**

4 **660 Figure 1:** Geographic location of the Dakhla peninsula, south of Morocco. (a), map of
5
6
7 **661** Morocco with principal towns; (b), location of the geological sections studied (stars). 1:
8
9 **662** Garitas, 2: Porto Rico, 3: El Argoub. The black circles denote the outcrops of interest along
10
11 **663** the Atlantic Ocean coast.

12
13
14 **664 Figure 2:** Stratigraphic section of the Garitas sedimentological sequence. U1-U5 refers to the
15
16 **665** unit and the number on the right of the column represents the lithofacies.

17
18
19 **666 Figure 3:** Field photographs showing: (a) a general view of the lower part of the Garitas
20
21 **667** section, horizontal heterolithic stratification; (b) a detail of A, showing blackish (A1) rich in
22
23 **668** organic matter levels; (c) a phosphorite rich organic matter with shark teeth (fossil-bearing
24
25 **669** level A1); (e) the beige marl and siliceous limestone with Neptunian dykes in (f).

26
27
28 **670 Figure 4:** Field photographs showing: (a) an example of coprolite level; (b) a succession of
29
30 **671** gray limestone bar and beige sandy calcareous marl (lithofacies 3 in figure 2), black to brown
31
32 **672** or dark siliceous limestone with coprolites at its base (lithofacies 4), yellowish sandy marl
33
34 **673** rich in vertebrate fossil, fossil-bearing level B1 (lithofacies 5); (c) a whitish marl with
35
36 **674** lenticular brown siliceous limestone (lithofacies 6).

37
38
39 **675 Figure 5:** Garitas section. (a) lithofacies 6 forms the prominent ledge; (b) overlaying muddy
40
41 **676** brown yellow sandstone corresponding to fossil-bearing level B2 (lithofacies 7).

42
43
44
45 **677 Figure 6:** Field photographs showing the top of the Garitas section with lithofacies 9, 10 and
46
47 **678** 11.

48
49
50 **679 Figure 7:** Porto Rico section. (a) general view of the lower part of the section with the fossil-
51
52 **680** bearing levels B1 and B2; (b) exposure of the Unit U3 corresponding to the lithofacies 3,
53
54 **681** which consists of a thick multicolor sandy marl series interstratified by sandstone with
55
56 **682** limestone concretions (we can see the position of fossil-bearing levels C1 and C2); (c)

1
2
3 683 photograph showing the abundant selachian teeth of the B2 level; (d) landmark level of
4
5 684 gastropods and oysters coquina.

6
7
8 685 **Figure 8:** field photographs and measured section of North Porto Rico and El Argoub areas.
9
10 686 (a) section located 2 km north of El Argoub village, (b, c) sections is about 6 km north of
11
12 687 Portorico. See the landmark level consisting of gastropod and oyster coquina at the lower part
13
14 688 of U4.

15
16
17
18 689 **Figure 9:** Outline correlation between cross sections from Garitas to El Argoub.

19
20
21 690 **Figure 10:** Porto Rico section and position of paleomagnetic sampling and the NRM
22
23 691 intensities plotted against lithostratigraphic position (right curve). Note the position of the
24
25 692 fossil-bearing B1, B2, C1 and C2.

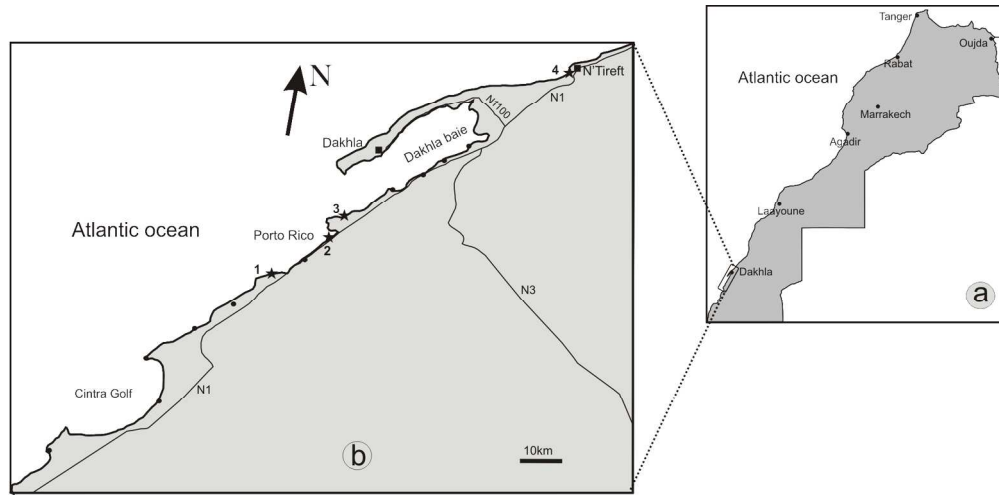
26
27
28 693 **Figure 11:** Paleomagnetic analysis: (a) acquisition of isothermal remanent magnetization
29
30 694 (IRM) (normalized values) curves of same samples, with most of the magnetization acquired
31
32 695 below 200 mT and saturation achieved at 300 mT; (b, c) stepwise thermal demagnetization of
33
34 696 the IRM components; (d) thermomagnetic curve of sample, where magnetic iron sulphides
35
36 697 where suspected to be present in the samples.

37
38
39
40 698 **Figure 12:** Demagnetization plots of the samples. The solid (open) symbols represent
41
42 699 horizontal (vertical) projections, respectively. (a) at 10 mT, the magnetization intensity fall
43
44 700 below the noise level of the magnetometer; (b) example of samples with erratic direction; (c)
45
46 701 example of samples with normal polarity from the site situated 2m above the C1 fossil-
47
48 702 bearing level; (d) equal area projection and Fisher statistics of the reliable characteristic
49
50 703 remanent magnetization (ChRM) direction. The 95% confidence ellipse for the normal (solid
51
52 704 star) mean directions is indicated (inclination=44.6°, declination=324.4°). Gray star is the
53
54 705 geocentric axial dipole of the Porto Rico latitude.

1
2
3 706 **Figure 13:** Carbon isotope values (‰ VPDB) of the Porto Rico and El Argoub sections,
4
5 707 compared to $\delta^{13}\text{C}$ curves around the Eocene-Oligocene transition in ODP Site 1218 (Erhardt et
6
7 708 al., 2013) and reference $\delta^{13}\text{C}$ composite curve (Cramer et al., 2009 modified by
8
9 709 Vandenberghe et al., 2012). EOT=Eocene-Oligocene Transition; U1 to U5 refer to the
10
11 710 lithological units defined in the text. B1, B2, C1 and C2 are fossil-bearing levels.
12

13
14
15 711 **Table 1:** Sample labels, CaCO_3 content (%) and $\delta^{13}\text{C}_{\text{org}}$ values (‰, VPDB); N.A.= not
16
17 712 analyzed.
18
19
20
21
22
23
24
25
26
27
28
29
30
31
32
33
34
35
36
37
38
39
40
41
42
43
44
45
46
47
48
49
50
51
52
53
54
55
56
57
58
59
60

Proof For Review



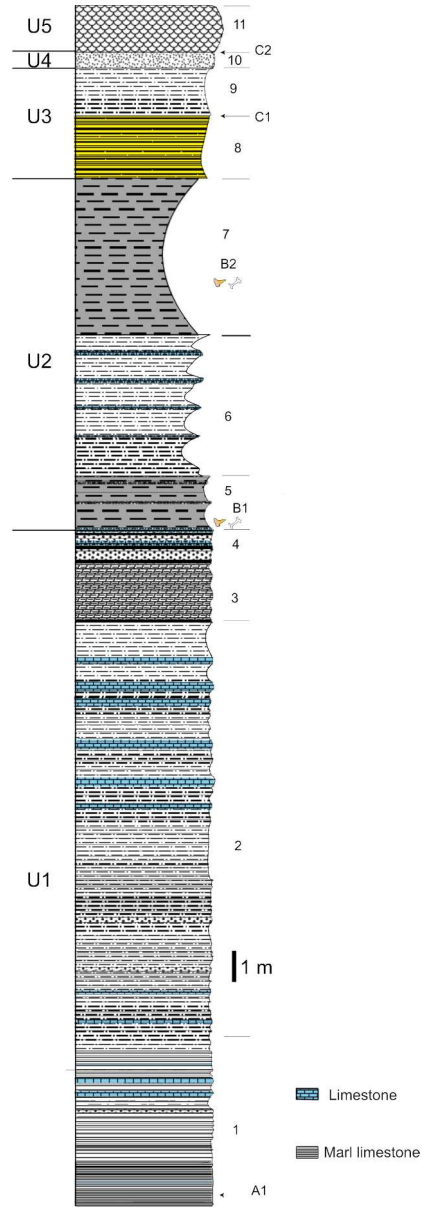
Geographic location of the Dakhla peninsula, south of Morocco. (a), map of Morocco with principal towns; (b), location of the geological sections studied (stars). 1: Garitas, 2: Porto Rico, 3: El Argoub. The black circles denote the outcrops of interest along the Atlantic Ocean coast.

169x83mm (300 x 300 DPI)

Or Review

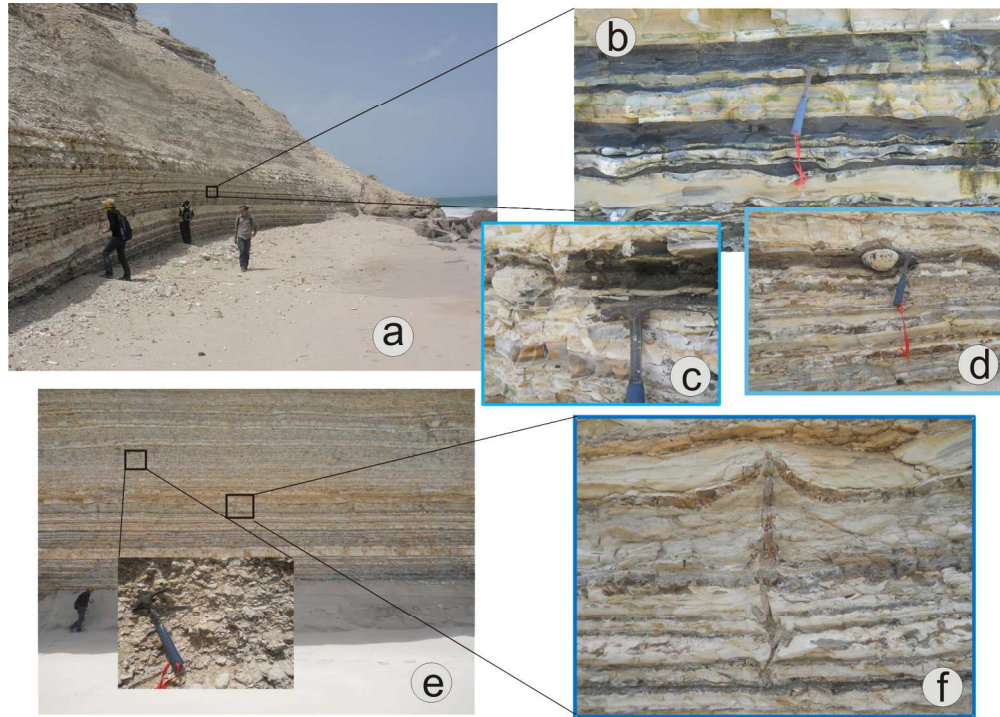
1
2
3
4
5
6
7
8
9
10
11
12
13
14
15
16
17
18
19
20
21
22
23
24
25
26
27
28
29
30
31
32
33
34
35
36
37
38
39
40
41
42
43
44
45
46
47
48
49
50
51
52
53
54
55
56
57
58
59
60

1
2
3
4
5
6
7
8
9
10
11
12
13
14
15
16
17
18
19
20
21
22
23
24
25
26
27
28
29
30
31
32
33
34
35
36
37
38
39
40
41
42
43
44
45
46
47
48
49
50
51
52
53
54
55
56
57
58
59
60



Stratigraphic section of the Garitas sedimentological sequence. U1-U5 refers to the unit and the number on the right of the column represents the lithofacies.

79x234mm (300 x 300 DPI)

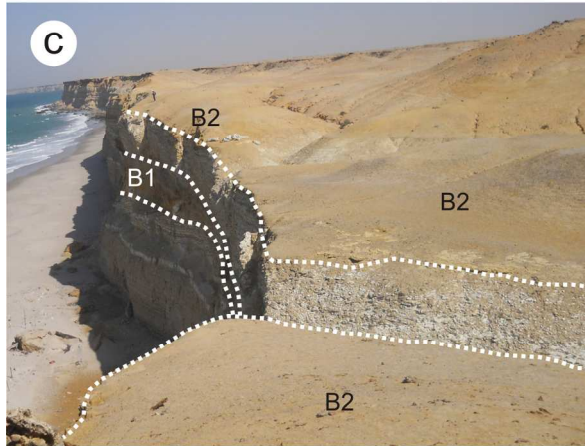
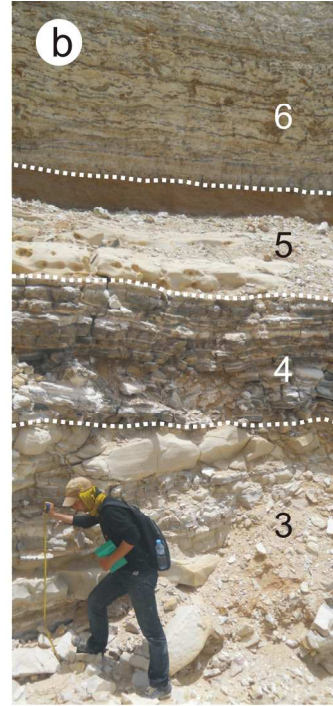


Field photographs showing: (a) a general view of the lower part of the Garitas section, horizontal heterolithic stratification; (b) a detail of A, showing blackish (A1) rich in organic matter levels; (c) a phosphorite rich organic matter with shark teeth (fossil-bearing level A1); (e) the beige marl and siliceous limestone with Neptunian dykes in (f).

169x121mm (300 x 300 DPI)

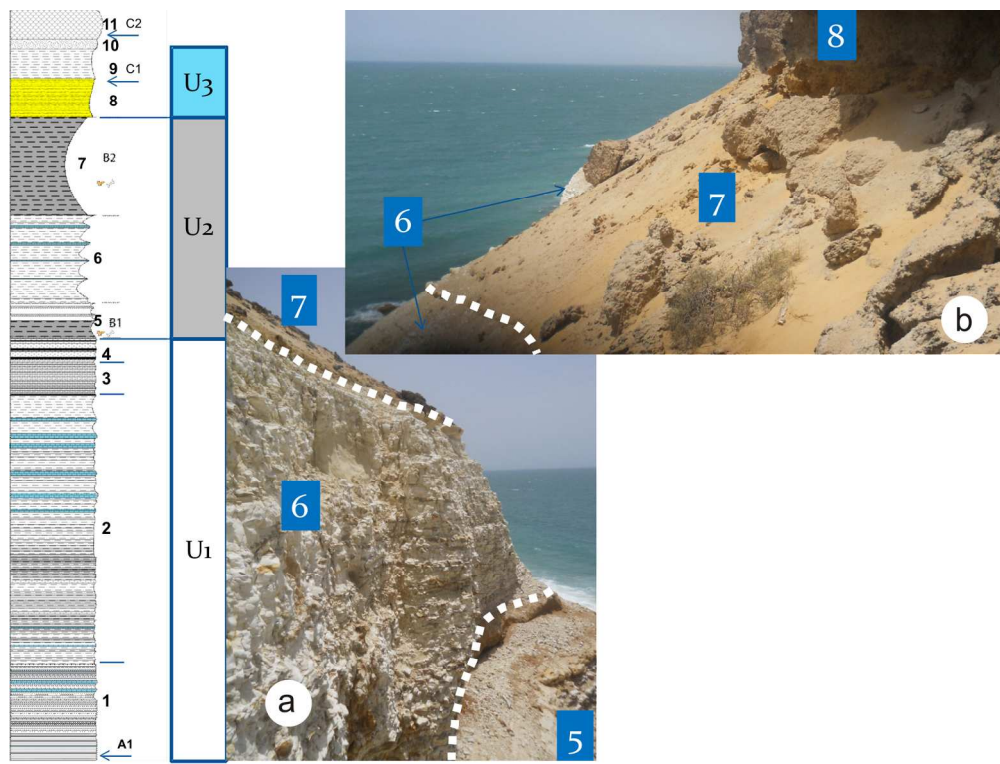
Review

1
2
3
4
5
6
7
8
9
10
11
12
13
14
15
16
17
18
19
20
21
22
23
24
25
26
27
28
29
30
31
32
33
34
35
36
37
38
39
40
41
42
43
44
45
46
47
48
49
50
51
52
53
54
55
56
57
58
59
60



Field photographs showing: (a) an example of coprolite level; (b) a succession of gray limestone bar and beige sandy calcareous marl (lithofacies 3 in figure 2), black to brown or dark siliceous limestone with coprolites at its base (lithofacies 4), yellowish sandy marl rich in vertebrate fossil, fossil-bearing level B1 (lithofacies 5); (c) a whitish marl with lenticular brown siliceous limestone (lithofacies 6).

170x122mm (300 x 300 DPI)



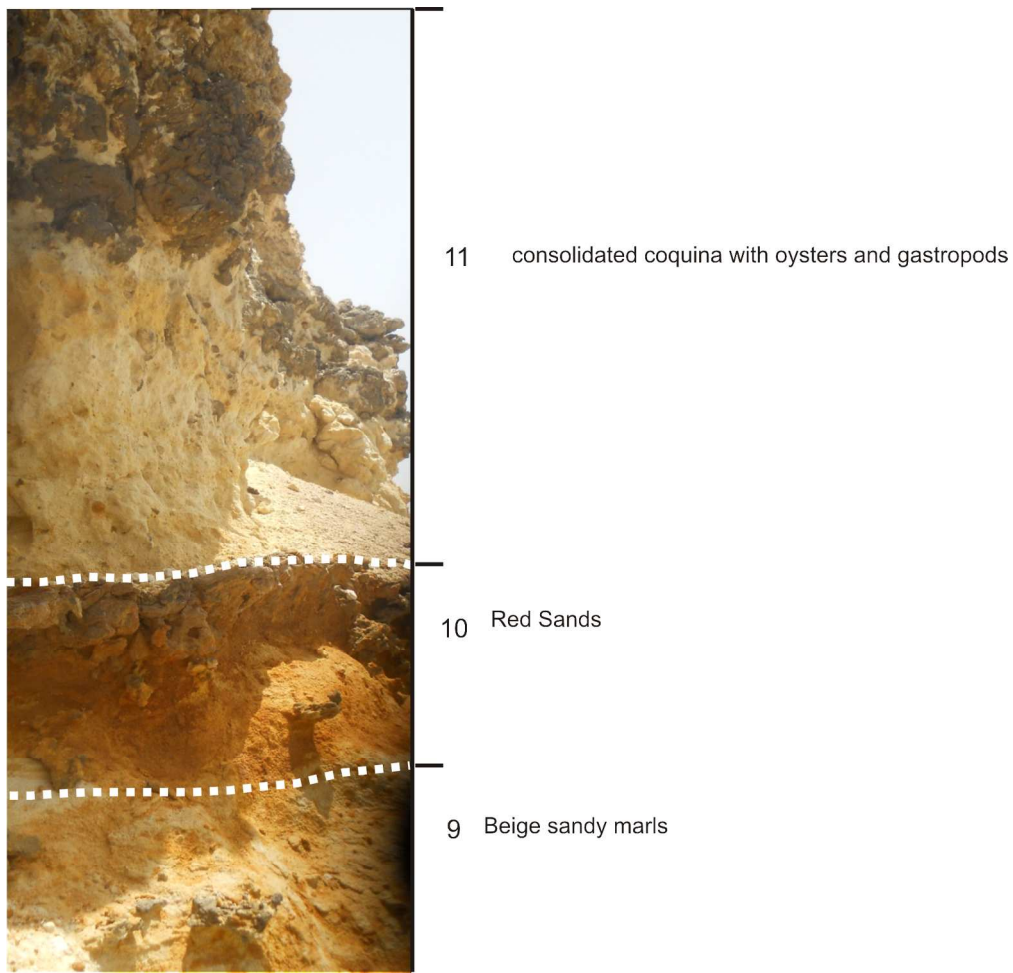
Garitas section. (a) lithofacies 6 forms the prominent ledge; (b) overlaying muddy brown yellow sandstone corresponding to fossil-bearing level B2 (lithofacies 7).

173x130mm (300 x 300 DPI)

review

1
2
3
4
5
6
7
8
9
10
11
12
13
14
15
16
17
18
19
20
21
22
23
24
25
26
27
28
29
30
31
32
33
34
35
36
37
38
39
40
41
42
43
44
45
46
47
48
49
50
51
52
53
54
55
56
57
58
59
60

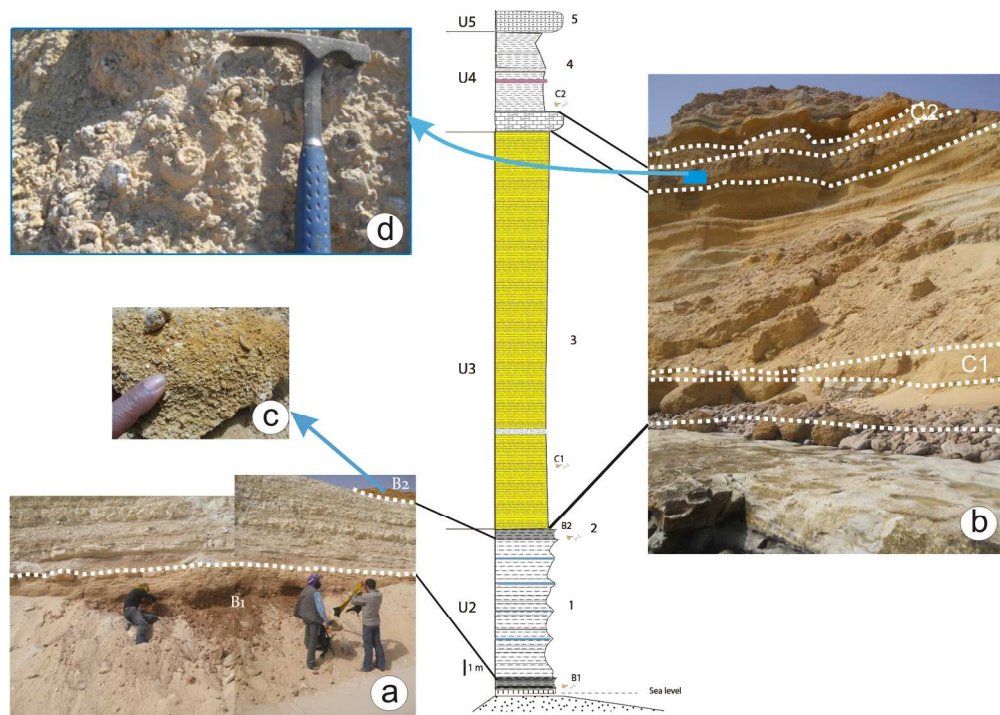
1
2
3
4
5
6
7
8
9
10
11
12
13
14
15
16
17
18
19
20
21
22
23
24
25
26
27
28
29
30
31
32
33
34
35
36
37
38
39
40
41
42
43
44
45
46
47
48
49
50
51
52
53
54
55
56
57
58
59
60



Field photographs showing the top of the Garitas section with lithofacies 9, 10 and 11.

169x163mm (300 x 300 DPI)



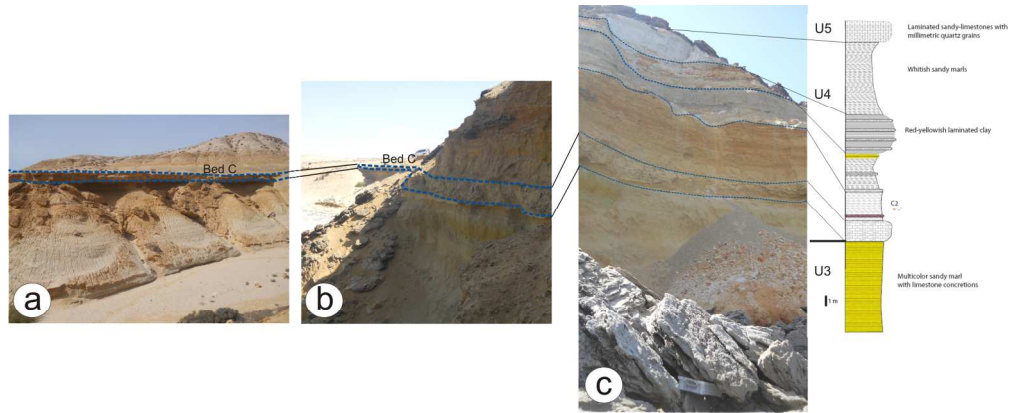


Porto Rico section. (a) general view of the lower part of the section with the fossil-bearing levels B1 and B2; (b) exposure of the Unit U3 corresponding to the lithofacies 3, which consists of a thick multicolor sandy marl series interstratified by sandstone with limestone concretions (we can see the position of fossil-bearing levels C1 and C2); (c) photograph showing the abundant selachian teeth of the B2 level; (d) landmark level of gastropods and oysters coquina.

170x120mm (300 x 300 DPI)

view

1
2
3
4
5
6
7
8
9
10
11
12
13
14
15
16
17
18
19
20
21
22
23
24
25
26
27
28
29
30
31
32
33
34
35
36
37
38
39
40
41
42
43
44
45
46
47
48
49
50
51
52
53
54
55
56
57
58
59
60

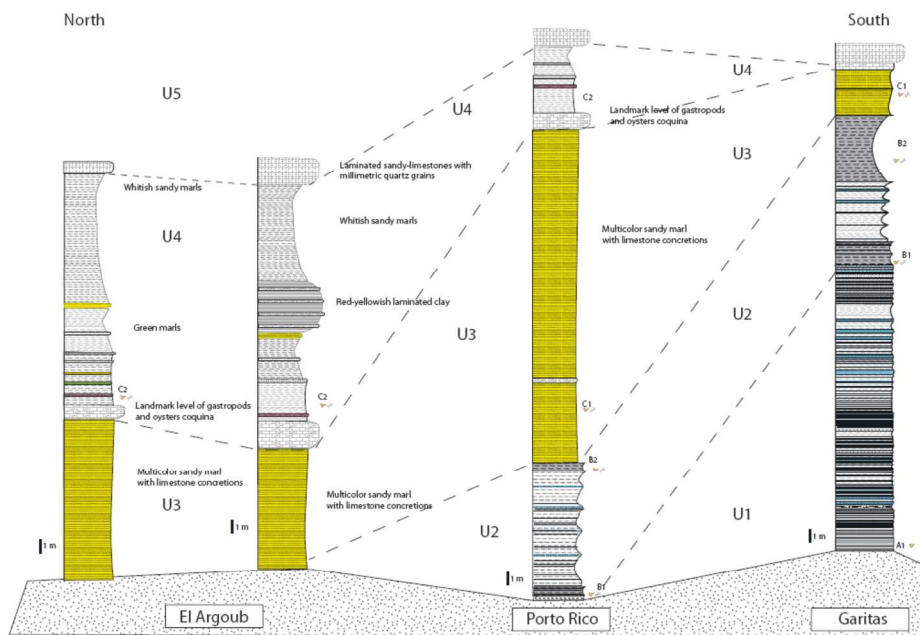


field photographs and measured section of North Porto Rico and El Argoub areas. (a) section located 2 km north of El Argoub village, (b, c) sections is about 6 km north of Portorico. See the landmark level consisting of gastropod and oyster coquina at the lower part of U4.

167x68mm (300 x 300 DPI)

For Review

1
2
3
4
5
6
7
8
9
10
11
12
13
14
15
16
17
18
19
20
21
22
23
24
25
26
27
28
29
30
31
32
33
34
35
36
37
38
39
40
41
42
43
44
45
46
47
48
49
50
51
52
53
54
55
56
57
58
59
60



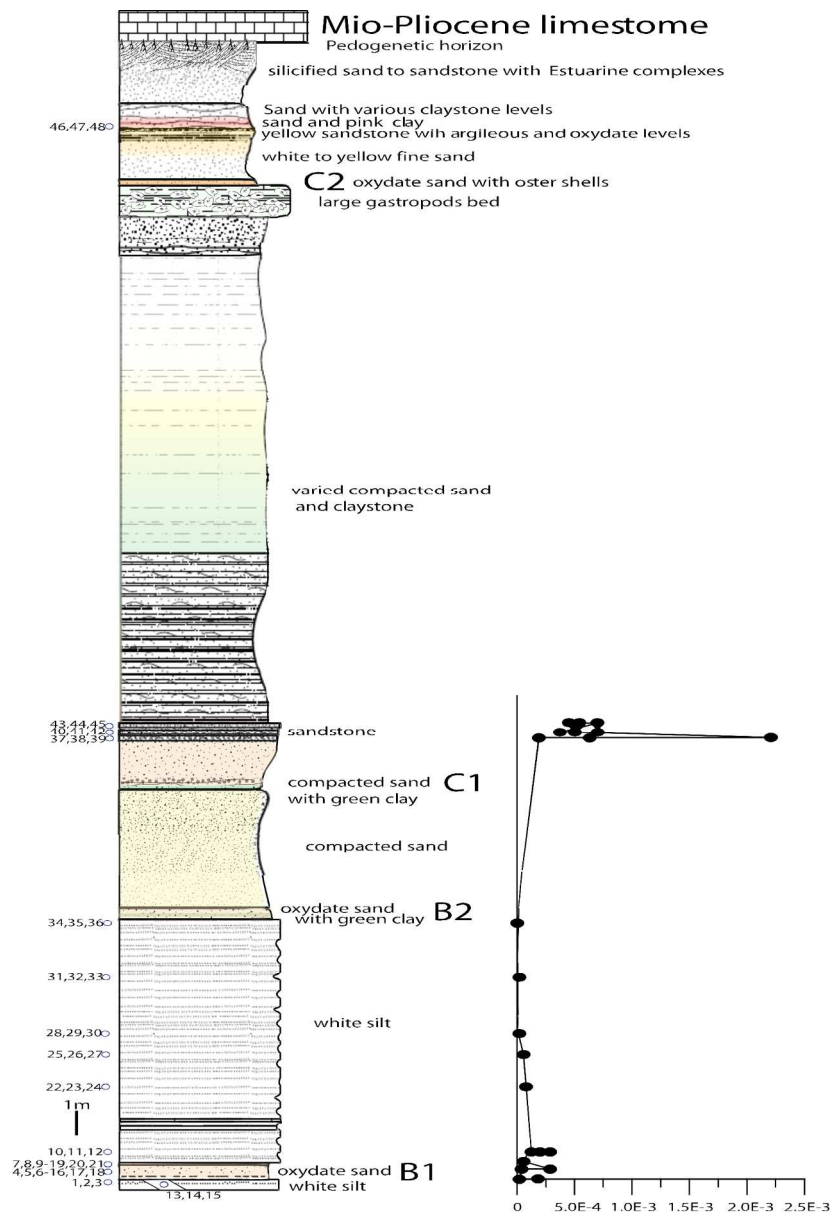
Outline correlation between cross sections from Garitas to El Argoub.

170x119mm (300 x 300 DPI)

Review

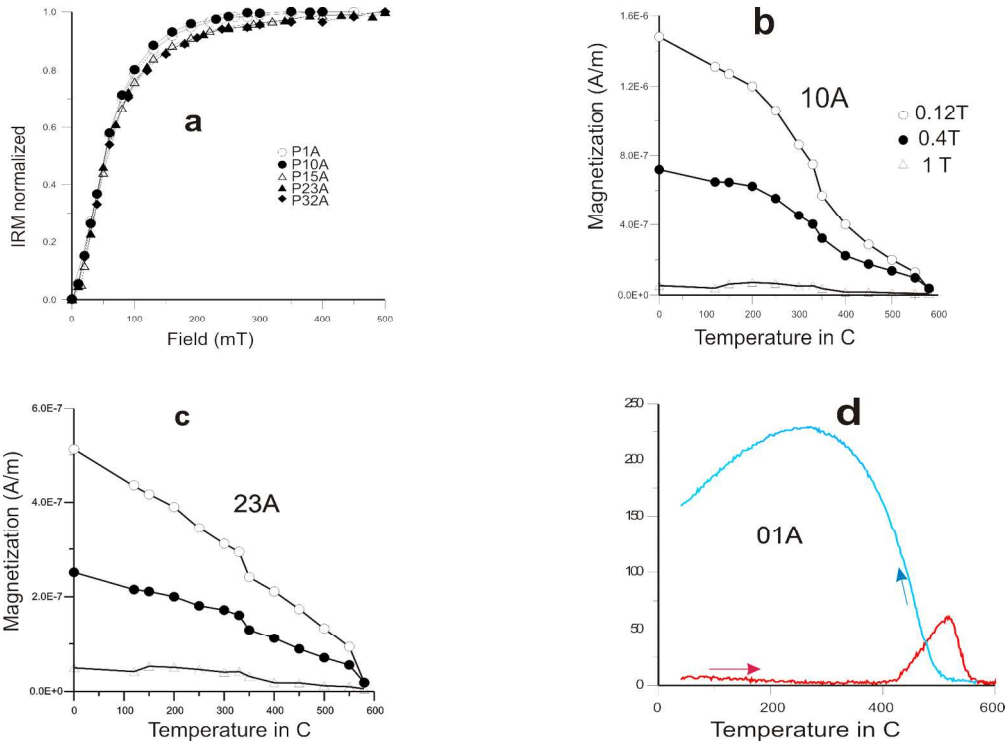
1
2
3
4
5
6
7
8
9
10
11
12
13
14
15
16
17
18
19
20
21
22
23
24
25
26
27
28
29
30
31
32
33
34
35
36
37
38
39
40
41
42
43
44
45
46
47
48
49
50
51
52
53
54
55
56
57
58
59
60

1
2
3
4
5
6
7
8
9
10
11
12
13
14
15
16
17
18
19
20
21
22
23
24
25
26
27
28
29
30
31
32
33
34
35
36
37
38
39
40
41
42
43
44
45
46
47
48
49
50
51
52
53
54
55
56
57
58
59
60



Porto Rico section and position of paleomagnetic sampling and the NRM intensities plotted against lithostratigraphic position (right curve). Note the position of the fossil-bearing B1, B2, C1 and C2.

158x232mm (300 x 300 DPI)

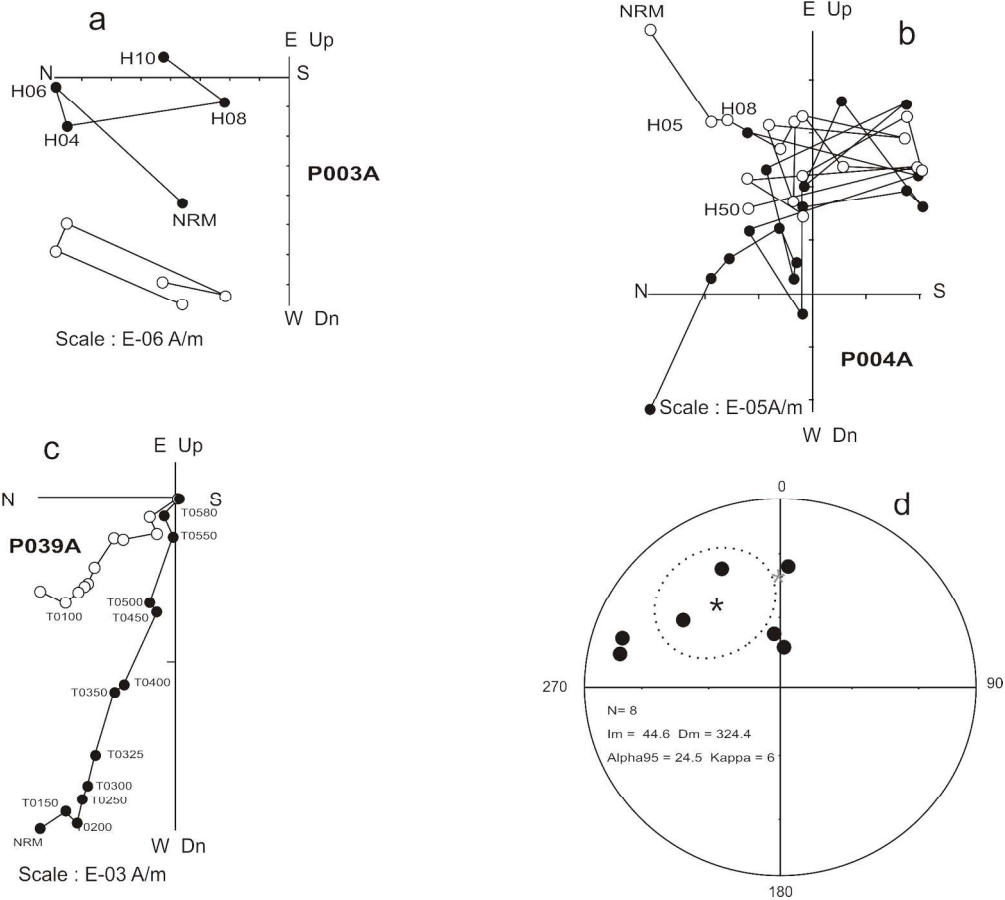


Paleomagnetic analysis: (a) acquisition of isothermal remanent magnetization (IRM) (normalized values) curves of same samples, with most of the magnetization acquired below 200 mT and saturation achieved at 300 mT; (b, c) stepwise thermal demagnetization of the IRM components; (d) thermomagnetic curve of sample, where magnetic iron sulphides were suspected to be present in the samples.

170x124mm (300 x 300 DPI)

view

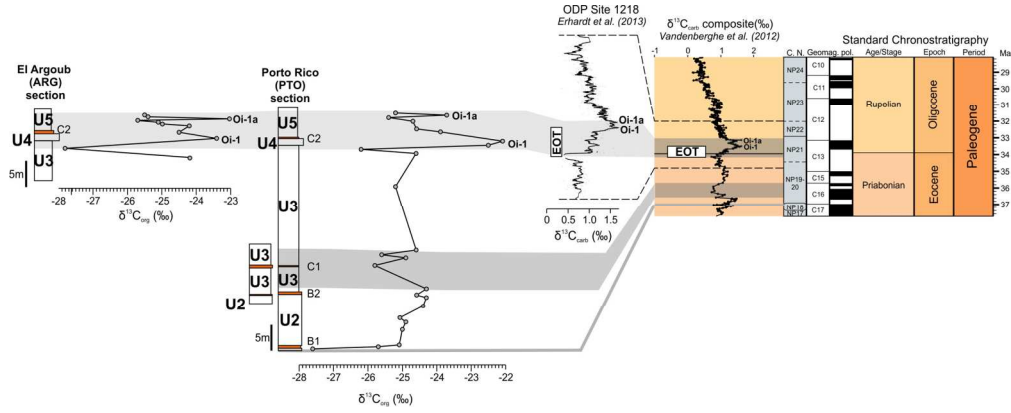
1
2
3
4
5
6
7
8
9
10
11
12
13
14
15
16
17
18
19
20
21
22
23
24
25
26
27
28
29
30
31
32
33
34
35
36
37
38
39
40
41
42
43
44
45
46
47
48
49
50
51
52
53
54
55
56
57
58
59
60



Demagnetization plots of the samples. The solid (open) symbols represent horizontal (vertical) projections, respectively. (a) at 10 mT, the magnetization intensity fall below the noise level of the magnetometer; (b) example of samples with erratic direction; (c) example of samples with normal polarity from the site situated 2m above the C1 fossil-bearing level; (d) equal area projection and Fisher statistics of the reliable characteristic remanent magnetization (ChRM) direction. The 95% confidence ellipse for the normal (solid star) mean directions is indicated (inclination=44.6°, declination=324.4°). Gray star is the geocentric axial dipole of the Porto Rico latitude.

170x152mm (300 x 300 DPI)

1
2
3
4
5
6
7
8
9
10
11
12
13
14
15
16
17
18
19
20
21
22
23
24
25
26
27
28
29
30
31
32
33
34
35
36
37
38
39
40
41
42
43
44
45
46
47
48
49
50
51
52
53
54
55
56
57
58
59
60



Carbon isotope values (‰ VPDB) of the Porto Rico and El Argoub sections, compared to $\delta^{13}C_{org}$ curves around the Eocene-Oligocene transition in ODP Site 1218 (Erhardt et al., 2013) and reference $\delta^{13}C$ composite curve (Cramer et al., 2009 modified by Vandenbergh et al., 2012). EOT=Eocene-Oligocene Transition; U1 to U5 refer to the lithological units defined in the text. B1, B2, C1 and C2 are fossil-bearing levels.

170x68mm (300 x 300 DPI)

For Review

1
2
3
4
5
6
7
8
9
10
11
12
13
14
15
16
17
18
19
20
21
22
23
24
25
26
27
28
29
30
31
32
33
34
35
36
37
38
39
40
41
42
43
44
45
46
47
48
49
50
51
52
53
54
55
56
57
58
59
60

section	label	CaCO ₃ (%)	δ ¹³ C _{org} (‰ VPDB)
Porto Rico section	PTO15-18	0.0	-25.2
	PTO15-17	0.0	-23.7
	PTO15-16	0.0	-25.4
	PTO15-15	0.0	-24.7
	PTO15-14	0.0	-24.6
	PTO15-13	0.0	-23.9
	PTO15-11	55.1	-22.1
	PTO15-10	1.0	-22.5
	PTO15-9	0.6	-26.2
	PTO15-8	5.0	-24.6
	PTO15-7	0.0	-25.2
	PTO15-5	0.0	-24.6
	PTO-41	2.0	-25.6
	PTO15-4	0.0	-25.0
	PTO15-3	0.0	-25.8
	PTO15-2	1.2	-24.3
	PTO-34	76.0	-24.6
	PTO15-1	76.9	-24.3
	PTO-32B	1.0	-24.4
	PTO-30B	1.0	-25.1
	PTO-26B	1.0	-24.9
	PTO-22B	2.0	-25.0
	PTO-21B	59.0	-25.1
PTO-16B	60.0	-25.7	
PTO-2	43.0	-27.6	
El Argoub section	ARG15-12	0.0	-25.5
	ARG15-11	0.0	-25.4
	ARG15-10	1.4	-23.0
	ARG15-9	1.3	-25.7
	ARG15-8	0.0	-25.1
	ARG15-7	1.0	-25.0
	ARG15-6	3.2	-24.2
	ARG15-4	45.3	-24.5
	ARG15-3	28.7	-23.4
	ARG15-2	0.0	-27.8
ARG15-1	0.5	-24.2	
Not analyzed (TOC too low)	PTO15-12	41.2	TOC too low
	PTO15-6	0.0	TOC too low
	ARG15-5	N.A.	TOC too low
	PTO-43	3.0	TOC too low
	PTO-19	N.A.	TOC too low
	PTO-11	19.0	TOC too low
PTO-5	N.A.	TOC too low	

Sample labels, CaCO₃ content (%) and δ¹³C_{org} values (‰, VPDB); N.A.= not analyzed.

210x297mm (200 x 200 DPI)